USGS
science for a changing world

Structure, Velocities, and Faulting Relationships Beneath San Gorgonio Pass, California: Implications for Water Resources and Earthquake Hazards

by

R. D. Catchings, M. R. Goldman, G. Gandhok, E. Horta, M. J. Rymer, P. Martin, and A. Christensen

Open-File Report 99-568

1999

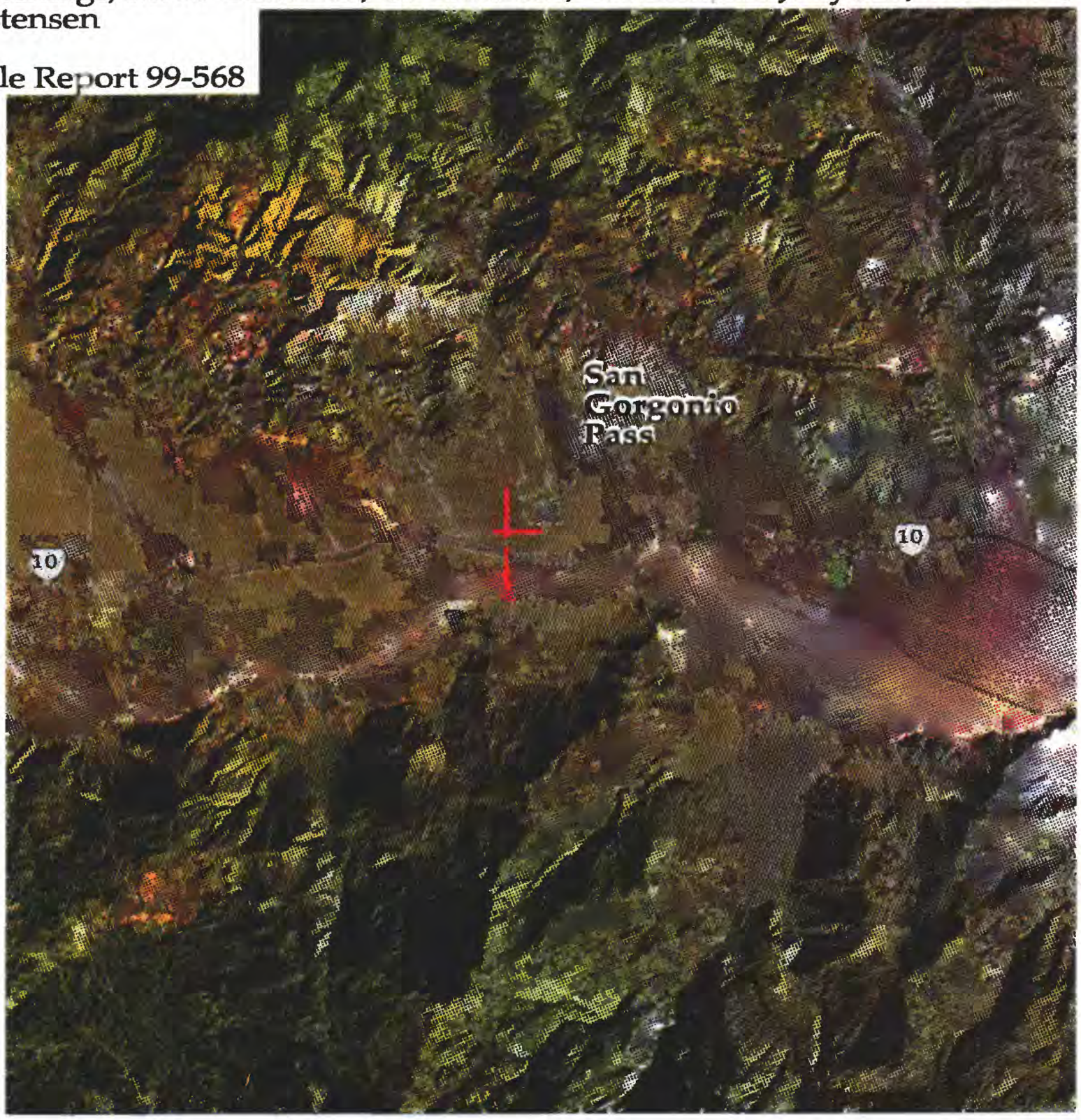

U. S. DEPARTMENT OF THE INTERIOR
U.S. GEOLOGICAL SURVEY

Menlo Park, California

Table of Contents

List of Tables

List of Figures

Introduction

San Gorgornio Pass, California is an east-west-trending, topographically low-lying area between the San Bernardino and the San Jacinto Mountains, located approximately 120 km east of Los Angeles (Fig. 1a). To investigate issues related to groundwater resources and earthquake hazards in the San Gorgonio Pass area, the USGS conducted a high-resolution seismic imaging investigation there in August 1997.

Groundwater is important to the region because small cities located within the Pass (including Beaumont, Cherry Valley, the Morongo Indian Reservation, and Cabazon) and cities east of the Pass (including Desert Hot Springs, Palm Springs, and Indio) obtain much of their water supply from groundwater that flows through the Pass. Some of the cities in San Gorgonio Pass supplement naturally occuring groundwater by injecting water obtained from the Colorado River aqueduct into the subsurface. Water injected and stored during wet periods (principally winter) is extracted during dry periods (principally summer), however, ground-water flow from the recharge area and within the Pass must be understood to maximize recovery of the stored water. Groundwater flow through the Pass cannot be accurately determined at present because there are few wells and the subsurface structure and stratigraphy in the area is not well known. Of the wells in the region, the well nearest to our seismic survey (Well MS-25) was located less than 20 meters from profiles SG 1 and 2 (Fig. 1a).

Earthquake hazards associated with San Gorgonio Pass are important locally to the cities within and near San Gorgorio Pass for obvious reasons, but these hazards are important to greater southern California because major lifelines (including transportation, water, gas, and electrical lifelines) to the larger urban areas west of the Pass trend through San Gorgorio Pass. The greatest hazard in the Pass may be associated with three major fault systems: the San Andreas to the north in the San Bernardino Mountains, the San Gorgonio Fault Zone within San Gorgonio Pass (Matti and Morton, 1993), and the San Jacinto to the south within the San Jacinto Mountains (Fig. 1b). Although the San Andreas and San Jacinto faults may be larger, with greater regional hazards, unknown faults within the San Gorgonio Fault Zone may be particularly disruptive to the infrastructure within the Pass and to lifelines trending through the Pass due to their close proximity.

The seismic investigation presented in this report benefits both water-resource and earthquake hazards investigations by: (1) mapping subsurface stratigraphic horizons that outline the groundwater flow system and whose structural configuration influences

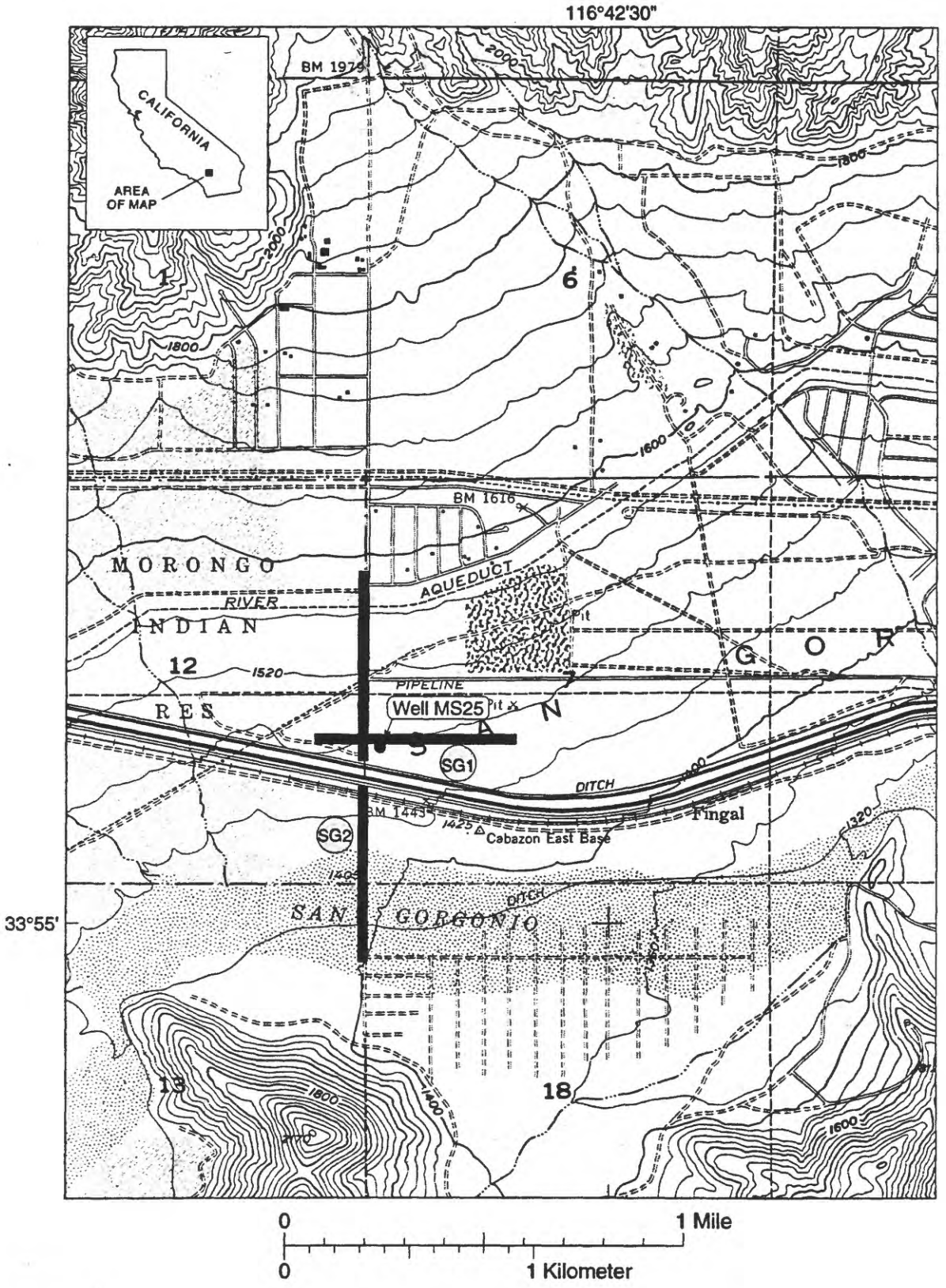

Figure 1a. Map of part of San Gorgonio Pass showing location of seismic lines (thick black lines) SG 1, oriented east-west, and SG 2, oriented north-south.

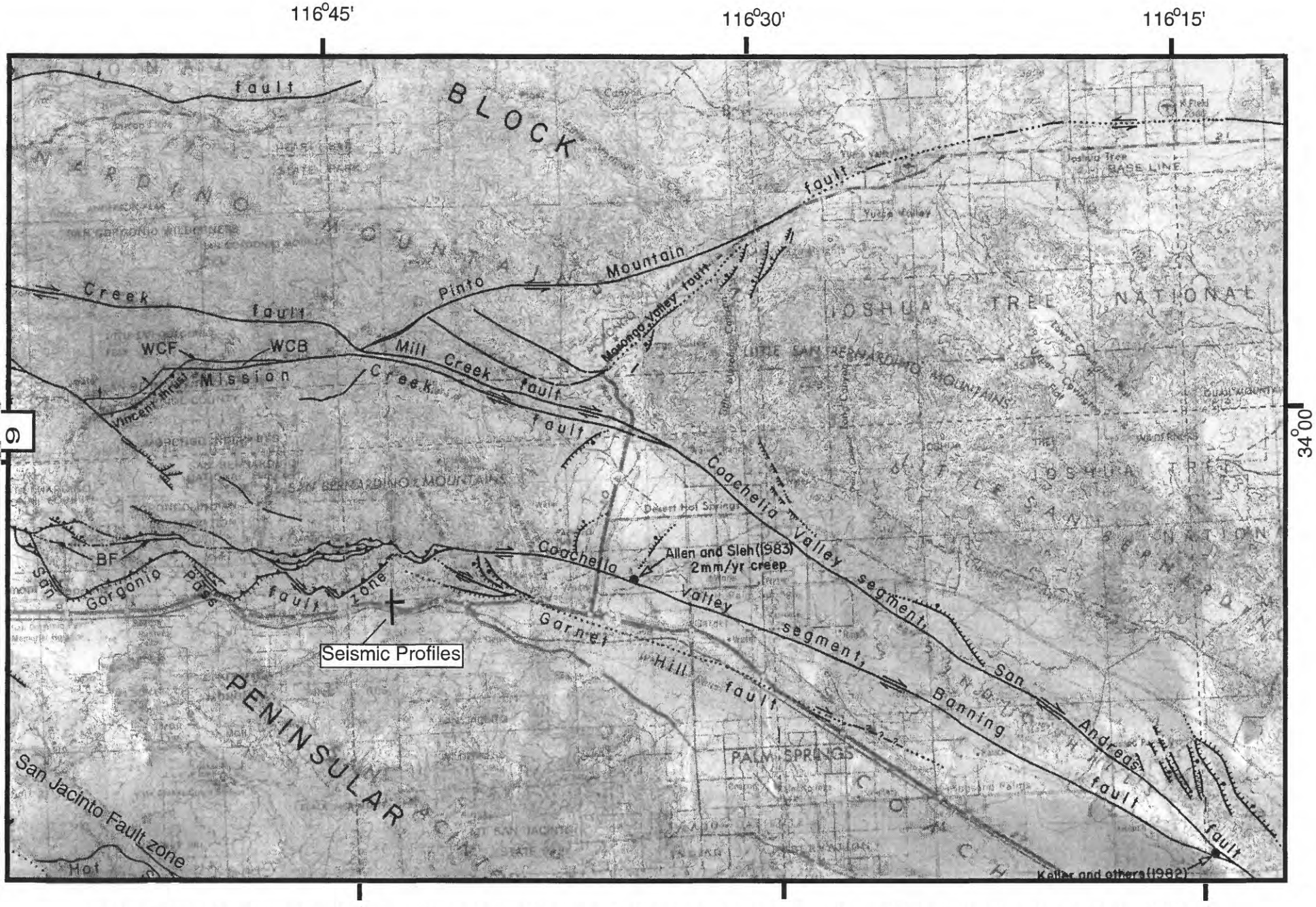

Fig. 1b Fault Map of the San Gorgonio Pass Area, Southern California with seismic profiles of this study (from Matti et al., 1992).

ground shaking during earthquakes, (2) measuring seismic velocities and and basin geometries associated with unconsolidated sediments, both of which influence groundwater flow as well as ground shaking, and (3) locating faults that represent potential seismic sources and perhaps influence groundwater flow.

Local Geology

The valley within San Gorgonio Pass is covered at the surface by Quaternary sediments that include Holocene and Pleistocene alluvial fan deposits and Holocene active channels and washes (Matti et al., 1992). Allen (1957) suggests that the entire sequence of sedimentary rocks from just below the surface to bedrock are Tertiary and Quaternary sediments derived from continental sources, except those rocks of the Imperial Formation, which are derived from northward incursion of marine waters into the Salton depression to the south. The stratigraphic sequence within the San Gorgorio Pass is summarized in Table 1.

The lithology within the San Bernardino Mountains to the north and the San Jacinto Mountains to the south consists largely of metamorphic rocks that have been intruded by plutonic rocks of quartz monzonitic composition (Allen, 1957). The intrusive dikes include pegmatite dikes, migmatitic rocks (granitic composition), and plutonic quartz monzonite rocks. Allen (1957) describes these rocks as a "hybrid of types of varying composition and transitional boundaries" that resulted from complex faulting within the San Bernardino Mountains. To the south, the crystalline rocks of the San Jacinto Mountains are largely Mesozoic, Paleozoic, and PreCambrian? granitoid and pre-batholithic metasedimentary rocks (Matti et al., 1992), consisting largely of quartzo-feldspathic gneisses and schists, hornblende schists, phyllite, crystalline limestone, and quartzite (Fraser, 1931). The metasedimentary rocks are underlain by intrusive rocks that are predominantly of granodiorite composition (Allen, 1957).

San Gorgonio Pass is located in a particularly complex area of the San Andreas Fault system. Southeast of San Gorgonio Pass, the San Andreas Fault is split into two segments, the Mission Creek segment which trends north of San Gorgonio Pass within the San Bernardino Mountains, and the Banning segment which trends largely along the southern end of the San Bernardino Mountains (Fig. 1b). The Banning fault may be up to 100 km in length and has generated as much as 16-25 km of right lateral slip since the Miocene, but in the San Gorgonio Pass area, the Banning fault has been modified by Quaternary reverse, thrust, and wrench faults, the assemblage of which Matti et al.(1992) call the San Gregonio Pass fault zone (Fig. 1b). Right-lateral movement apparently

Table: 1. Sequence and character of the Sedimentary rocks of San Gorgonio Pass (Allen, 1957).

Formation	Age	Max.thickness (feet)	Lithology
Alluvium	Recent		Unconsolidated stream gravels and low stream terrace gravels
-Unconformity-	----------		
Landslide deposits	Recent		
-Unconformity-	----------		
Undifferentiated terrace gravels	Quaternary		Terrace gravel and canyon-fill material of doubtful correlation
-Unconformity-	----------		
Burnt Canyon breccia	Quaternary	100 +	Dissected landslide deposit
-Unconformity-	----------		
Heights Fanglomerate	Quaternary	500	Tan to dark-brown, ill-sorted conglomerate, dominantly dark clasts of gneissic rock
-Unconformity-	----------		
Cabezon Fanglomerate	Quaternary	1500 +	Grey to tan ill-sorted conglomerate, rich in clasts of pegmatitic and granitic rocks
-Unconformity-	----------		
Deformed gravels of Whitewater river	Quaternary (?)		Grey to tan ill-sorted conglomerate, rich in clasts of pegmatitic and granitic rocks
-Contact not exposed-	----------		
San Timoteo Formation (?)	Pliocene-Pleistocene	1800 +	Tan to grey sandstone, siltstone, and conglomerate, rich in light-coloured clasts of granitic rocks; interbedded fresh water limestone
-Contact not exposed-			
Painted Hill Formation	Middle Pliocene ?	3400 +	Light-grey sandstone and conglomerate, rich in clasts of volcanic and granitic rocks:Ppc, resistant conglomerate bed;Ppb, interlayered flows of olivine basalt;Ppd, associated dykes
Imperial Formation	Lower Pliocene ?	300	Tan to yellow marine sandstone, siltstone, and shale;fossiliferous
Hathaway Formation			
Upper Member	Lower Pliocene ?	650	Grey, massive, ill-sorted conglomerate and brecchia, rich in clasts of augen and flaser gneiss
Lower Member	Lower Pliocene ?	1100 +	Light-grey sandstone, siltstone, conglomerate, and fresh-water limestone
Contact not exposed--			
Coachella fanglomerate			massive conglomerate, locally rich in clasts of basalt and dark-green gneiss;Mcb,interlayered flows of olivine basalt;Mcd, associated dykes:Mcm, marker horizon
Upper Member	Upper Miocene ?	3750 +	containing distinctive clasts well-indurated masisve conglomerate, locally rich in clasts of
Lower Member	Upper Miocene ?	850	olivine basalt:basal brecchia of grey schist fragments

continues near the southern end of the Banning fault and may be the source of the 1986 M=5.9, North Palm Springs earthquake, but the westernmost segment of the Banning fault may be inactive, as there is little evidence of ground ruptures during the Quaternary (Matti et al., 1992).

Understanding the complex faulting relationship within the San Gorgonio Pass region is made more difficult by the alluvial cover. Seismic studies, such as the one reported here, may help delineate some of the faulting relationships within the San Gorgonio Pass region.

Seismic Survey

Data Acquisition

In August 1997, the U. S. Geological Survey acquired two high-resolution seismic reflection and refraction profiles in San Gorgonio Pass (Fig. 1a,b). The seismic profiles (labeled SG 1 and SG 2) ranged in length from approximately 810 m to about 1577 m (Table 2). SG 1 was oriented approximately east-west, and SG 2 was oriented approximately north-south. The data were acquired using a shoot-through method, whereby, the geophones (i.e. the recording channels) remained stationary as shots were fired along the array. Approximately 4 seconds of data were recorded using a linear array of two to four Geometrics Strataview RX 60 ™ seismographs, each with 60 active channels. The data were stored on the hard drive of the seismograph during field acquisition and was later downloaded to 4 mm tape for permanent strorage in SEG-Y format.

Single-element, 40-Hz, vertical-component Mark Products L-40A ™ geophones were spaced at 5 m along each of the profiles. Seismic sources consisted of explosive 1-lb ammonium nitrate charges in ~2-m deep-holes and were spaced at 10-m intervals along the profile. The sources were co-located with geophones at 1-m lateral offsets. Seismic sources and seismographs were triggered simultaneously by synchronized electronic clocks with accuracies of approximately 1 ms.

Prior to acquiring the data, each recording site and shot point was measured with a meter tape and flagged to obtain the proper spacing. After the data were acquired, we used an electronic distance meter (EDM) to measure the recording sites and shot point locations with accuracies as great as 0.001 m.

Table 2. Acquisition parameters for San Gorgonio Pass seismic profiles. Distances are relative to the first shot point.

Profile #	Orientation	Length of Geophone Profile (m)	Length of Shot Point Profile (m)	No. of Shots	No. of CDP's	Maximum Fold
SG 1	W-E	594.99	810.22	80	281	59
SG 2	S-N	1297.62	1577.41	135	576	119

Shot and Geophone Locations

Variations in shot point and geophone locations and elevations can cause appreciable difficulty in stacking seismic reflection data and in accurately measuring the velocities if these variations are not included in processing the data. Large variations in line geometry may also result in data artifacts that are interpreted as structure. Therefore, we present the line geometries (see Appendices A-B) to aid in interpretation and reprocessing the seismic data.

To correlate seismic velocities and images with possible geometrical variations in the profile, we present graphical displays of the geometry along each profile, including shot point and geophone elevations, lateral variations from straight lines of shot point and geophone arrays, and fold (described below). In many instances, abrupt changes in elevation can be correlated with faults or major changes in stratigraphy, but apparent faults or stratigraphic changes that correlate with significant or abrupt changes in shot point and geophone arrays or large jumps in fold may also be artifacts.

Seismic Data Processing

Both reflection and refraction data were available because the data were acquired using a shoot-through configuration. This type of data acquisition has numerous advantages over conventional data acquisition because detailed velocity data are available and folds are typically much greater for reflection stacks.

Seismic Refraction Velocity Analysis

For refraction data processing, we used a seismic tomographic inversion method developed by Hole (1992), whereby, first arrivals on each seismic trace were used to measure detailed velocities from depths ranging from about 1 m to approximately 300 m

below the surface. For greater depths, velocities needed in seismic reflection stacking were determined using semblence and parabolic methods and from apriori knowledge of the local geology. As described below, we used the velocities derived from these methods to convert the reflection time-images to depth-images and, where necessary, to migrate the seismic reflection images.

Seismic Reflection Processing

Seismic reflection data processing was accomplished on a Sun Sparc 20 ™ computer using an interactive seismic processing package known as ProMAX™. The following steps were involved in data processing:

Geometry Installation

Lateral distances and elevations described above were used to define the geometrical set up of each profile. We installed the electronically-measured geometries into the ProMAX™ processing package for each profile separately so that shot and receiver elevations and locations could be included in the processing routine.

Trace Editing

Occasionally, bad coupling between the geophones and the ground, malfunctioning geophones, or cultural noise close to some seismic receivers resulted in unusually noisy traces at those locations, however, these traces were not unsuitable for all shot gathers. Therefore, independent trace editing was employed for each shot gather.

Bandpass Filtering

Most of the data of interest for seismic imaging and velocity measurement are well above 25 Hz, and most of the undesirable seismic data, such as surface waves and shear waves, were well below 25 Hz. Therefore, a bandpass filter with a low cut of 25 Hz was used to remove most surface and shear waves and cultural noise.

F-K Filtering

Not all surface waves were removed by simple bandpass filtering. To remove those surface waves and air waves that were not removed by bandpass filtering, we used a FK filter.

Timing Corrections

Although the shotgun source electronically triggers the seismographs, there are small (~2 ms) delays between the electrical trigger and the actual shotgun explosions. We corrected for the delays by removing a constant 2 ms from the start time of each shotgather.

Velocity Analysis

Velocities in the shallow section (~1 m to ~150 m) were determined using velocity inversion techniques, but velocities in the deeper section were determined using shotgathers and CDP stacks.

Elevation Statics

Elevation statics were also employed to correct for variations in elevations using locations derived from electronic measurements and velocities derived from the refraction velocity analysis.

Moveout Correction

Due to progressively greater traveltimes for the seismic waves to reach sensors that were progressively farther from each shot point, there was a delay (moveout) for each seismic arrival on the seismic record. To sum (stack) the data at each common depth point (CDP), a correction was made for the moveout using velocities obtained from the velocity analysis.

Velocity Inversion

Velocities were measured from first arrivals of the seismic data using a computerized inversion routine developed by Hole (1992).

Muting

To remove refractions and other arrivals that were not completely removed using filtering techniques, we used trace muting before and after stacking.

Stacking

To enhance the seismic signal at each location, individual reflections were summed together in a process called stacking.

Depth Conversion

For stacked seismic reflection sections that were not migrated, we converted the time sections to depth sections using RMS velocities converted from the velocity analysis described above in the velocity section.

Migration

Due to the presence of numerous faults and diffraction points in the subsurface, diffraction hyperbolae were observed throughout the section. We used pre-stack migration to collapse the diffraction hyperbolae to better identify the major faults.

Seismic Data

Profile SG 1

Profile SG 1 was oriented approximately east-west and extended 810 m parallel to Interstate 10 (Fig. 1a). Two RX-60 seismographs with 120 live channels were utilized to record the data. Geophones and shots were spaced at 5-m and 10-m intervals ,

respectively. A shot was fired adjacent to every other geophone (laterally offset by 1 m), and 11 shots were fired at each end of the recording array. Due to cultural features along the line (such as gas and utility lines), two shot point locations were not utilized along the seismic profile.

Geophones varied in elevation by no more than 7 m along the seismic profile, with elevations decreasing from west to east along the profile (Fig. 2). On seismic reflection sections, elevation is plotted relative to the topographically lowest geophone along the recording array, but because velocity information is available along the variation in topography, reflections along the topographic variation were included in the seismic reflection sections (e.g, no datum with reflections above topography removed). The geophone array varied by about 2 m from a straight line connecting the endpoints of the shotpoint array (Fig. 3); thus, relative to the entire length of the geophone array (~595 m), there was only about a 0.33% variation from a straight line. Therefore, it is unlikely that geometrical variations in the geophone array would cause artifacts in the data.

As the shot point array extended beyond the ends of the geophone array, the maximum variation in shot point elevations was greater than that of the geophone array. Shot point elevations varied by about 12 m along the shot-point array (Fig. 4), and relative to a straight line connecting the endpoints of the shot point array, shot points varied by about 2 m (Fig. 5). In terms of percentage of the entire length of the shot-point array, the 2-m variation in linearity is about 0.25%, which is far too little to cause artifacts in stacked sections.

Fold, (the theoretical number of times a reflection occurs at a given location) along SG 1 was smoothly varying because of the stationary recording array (Fig. 6). Maximum fold of about 59 was obtained near the center of the seismic profile and decreased to about 1 at the ends of the profile. Because maximum folds were near the middle of the seismic profile, the deeper structure is most reliably imaged near the center of the profile. However, the explosive sources used generate signals that are ususally strong enough to provide clear reflections to depths in excess of about 1 km with folds of about 1.

Profile SG 2

Profile SG 2 was oriented approximately south-north and extended 1577 m from near the northern end of the San Jacinto Mountains to just beyond the Colorado River aqueduct, north of Interstate 10 (Fig. 1a,b). Four RX-60 seismographs with 240 live channels were utilized to record the data. Geophones and shots were spaced at 5-m and 10-m intervals, respectively, with shot points laterally offset by 1 m from every second geophone (10 m). A total of 135 shots were fired into the array, but there were about 24

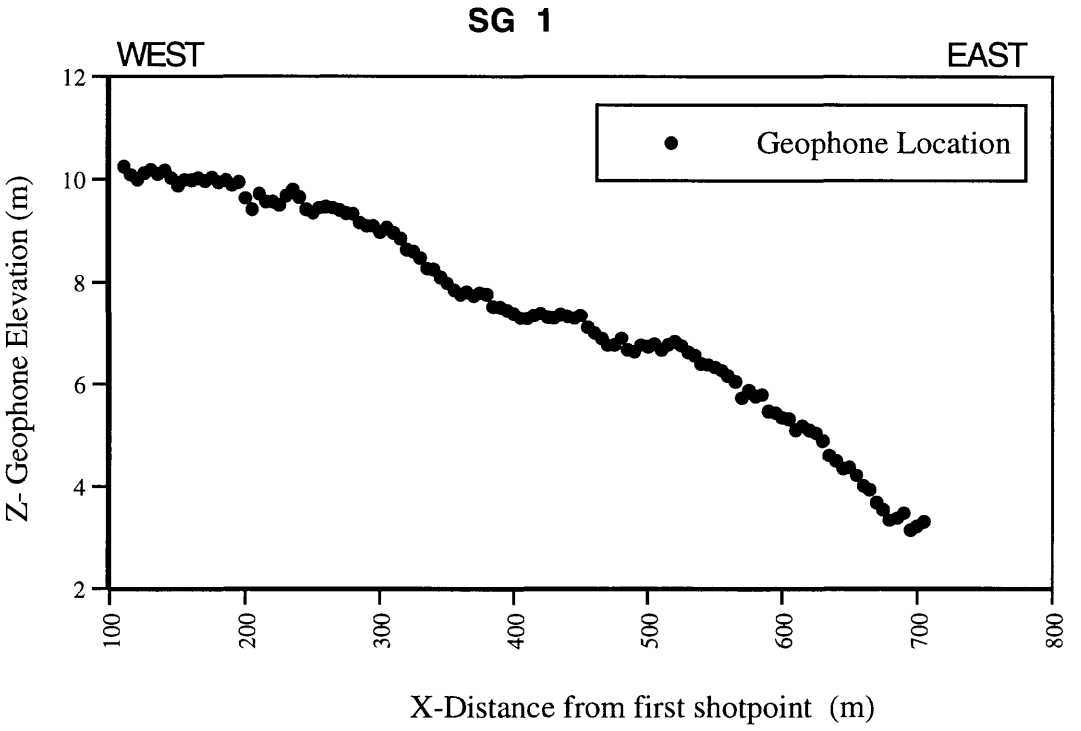

Figure 2. Geophone elevation along SG 1. Elevation is relative to the topographically lowest shotpoint.

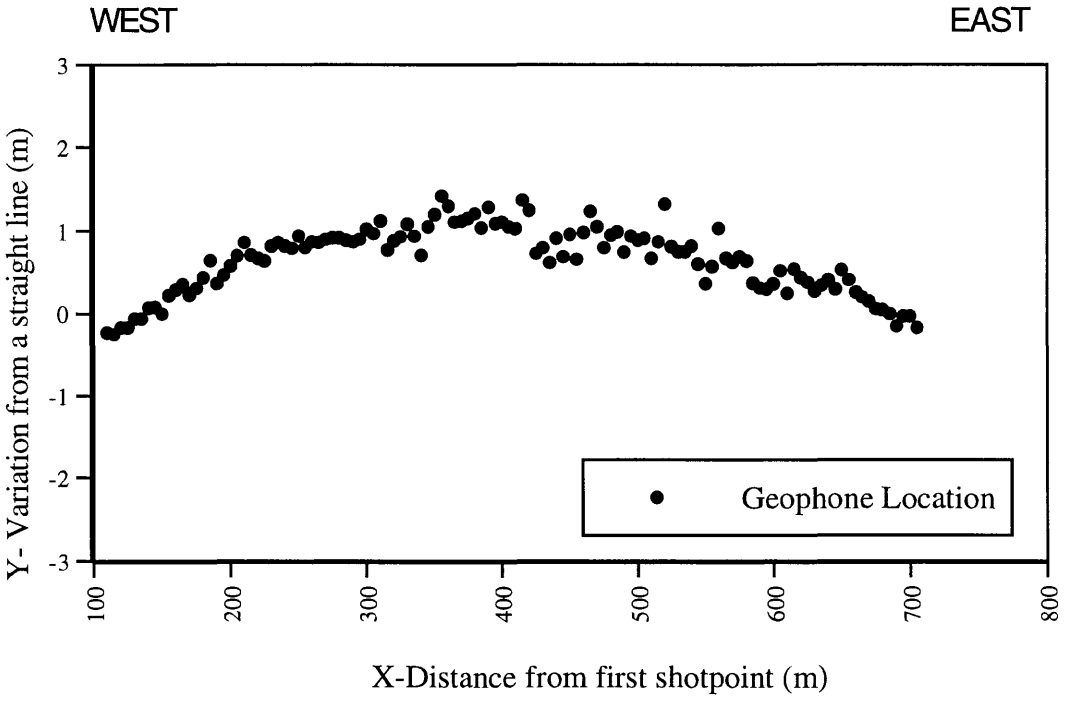

Figure 3. Geophone variation from a straight line connecting the first and last shot point along SG 1.

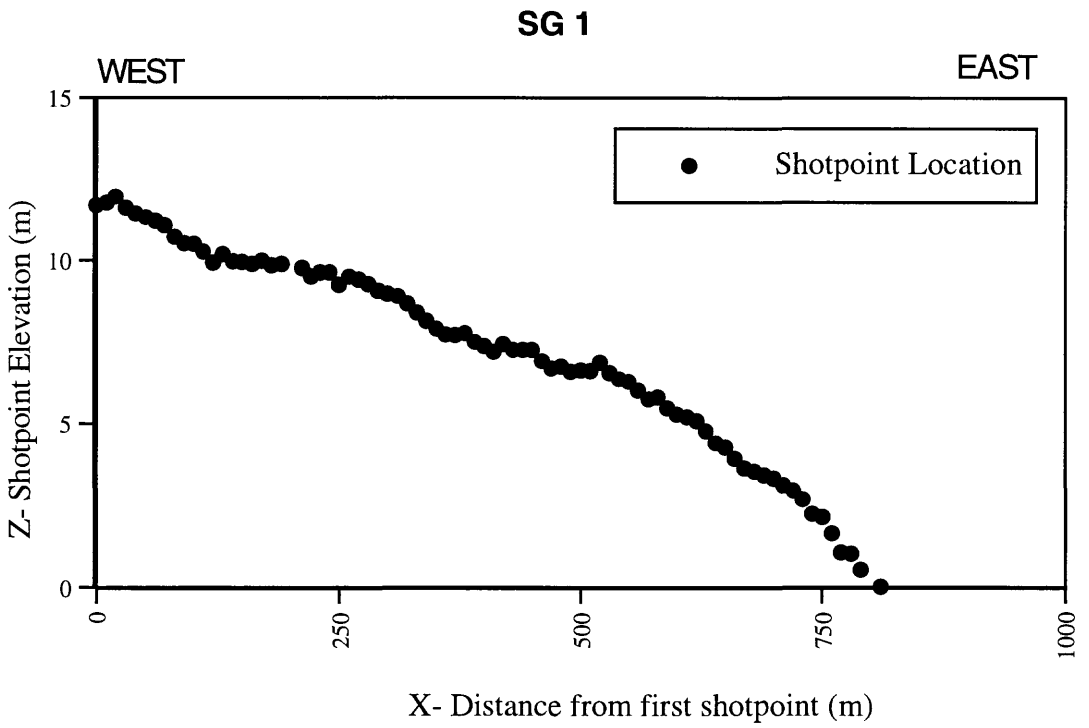

Figure 4. Shotpoint elevation along SG 1. Elevation is relative to the topographically lowest shotpoint.

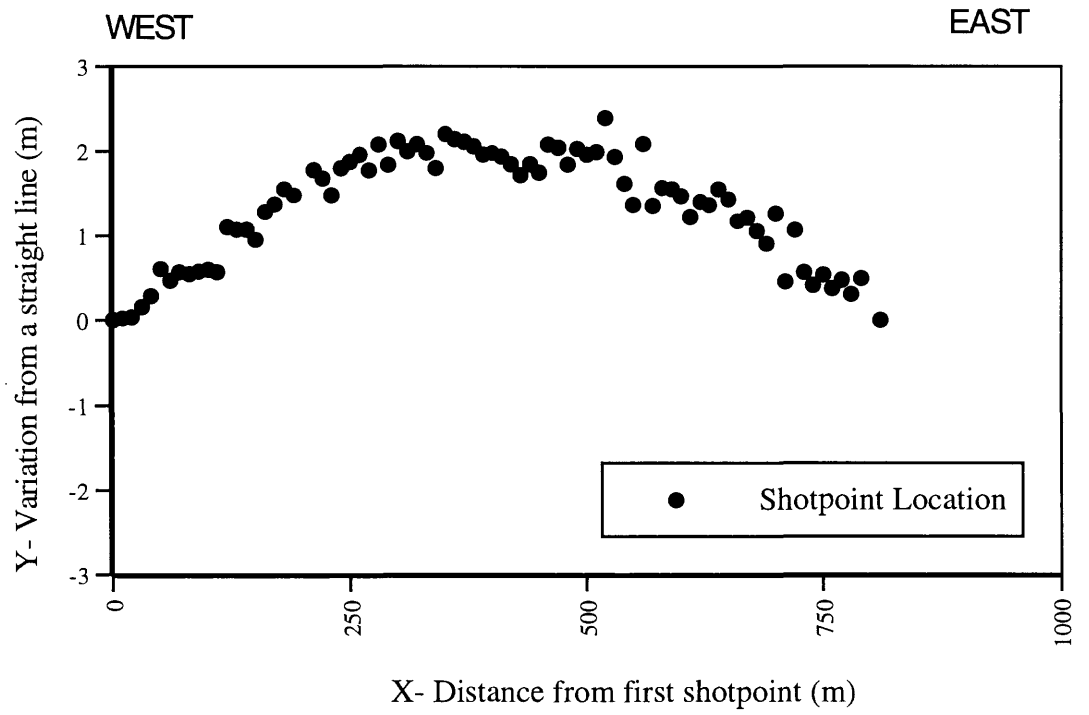

Figure 5. Shotpoint variation from a straight line connecting the first and last shotpoint along SG 1.

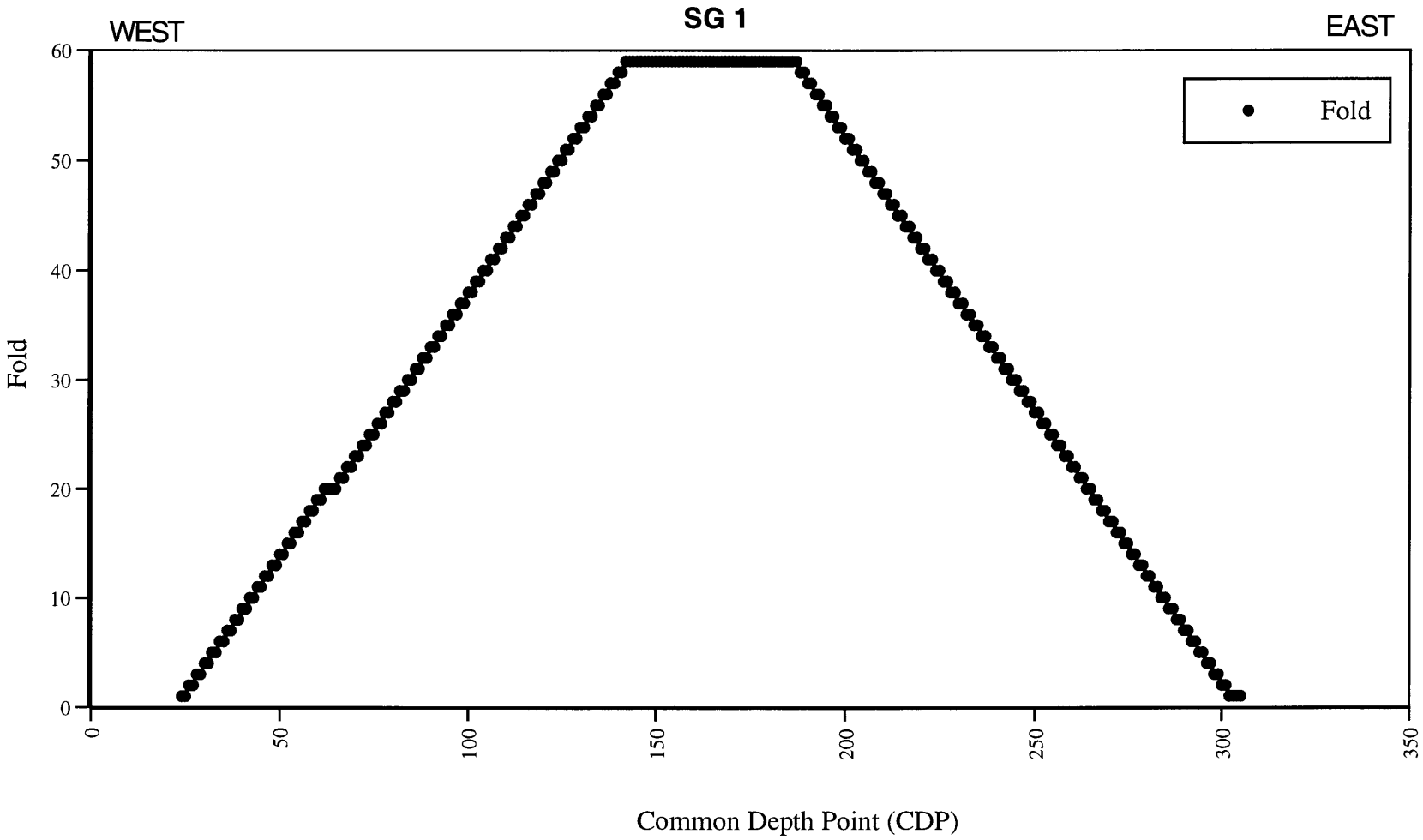

Figure 6. Fold as a function of common depth points along the seismic line. Distance is relative to the first shotpoint at the western end of the line.

shot points that were not used because of cultural features (such as the I-10 freeway, utilities, etc).

Geophones varied in elevation by about 50 m along the seismic profile, with elevations increasing from south to north along the profile (Fig. 7). On seismic reflection sections, elevation is plotted relative to the topographically lowest geophone along the recording array, but reflections along the topographic variation were included in the seismic reflection sections (e.g, topography above the datum was included with measured velocities). The geophone array varied from a straight line connecting the endpoints of the shot point array by a maximum of about 6 m (Fig. 8); thus, relative to the entire length of the seismic geophone array (~1300 m), there was only about a 0.54% variation from a straight line. It is unlikely, therefore, that geometrical variations in the geophone array would generate artifacts in the data that could be interpreted as structure.

Profile SG 2 included shot points that extended beyond the ends of the geophone array. On the northern end of the seismic profile, additional shot points were placed north of the California Aqueduct. These additional shot points resulted in a slightly greater elevation variation of the shot-point array relative to the geophone array, with a maximum elevation variation in excess of 55 m (Fig. 9); thus, the maximum variation in shot point elevations were greater than those of the geophone array. Shot points north of the Colorado River aqueduct could not be placed in line with the rest of the shot point array due to cultural features. When those additional shot points are included, relative to a line connecting the endpoints of the shot point array, shot points varied by about 15 m (Fig. 10). In terms of percentage of the entire length of the shot-point array, the 15-m variation in linearity is about 0.95%, which is probably too little to cause artifact in stacked sections. However, there is about a 10 m change in the linearity of the shotpoint array over a distance of about 100 m north of the aqueduct. Such a large change could cause artifacts in the data. Therefore, caution must be used interpreting structures in that part of the seismic profile.

Fold along SG 2 varies linearly along most of the seismic profile, but there are variations at several locations, due largely to skipped shot points (Fig. 11). Maximum fold of 119 was obtained near the center of the seismic profile and decreased to about 1 near the ends of the profile. Maximum folds greater than 100 likely generates strong signals to depths in excess of several kilometers, and fold of about 1 may generate strong signals to depths in excess of 1 km.

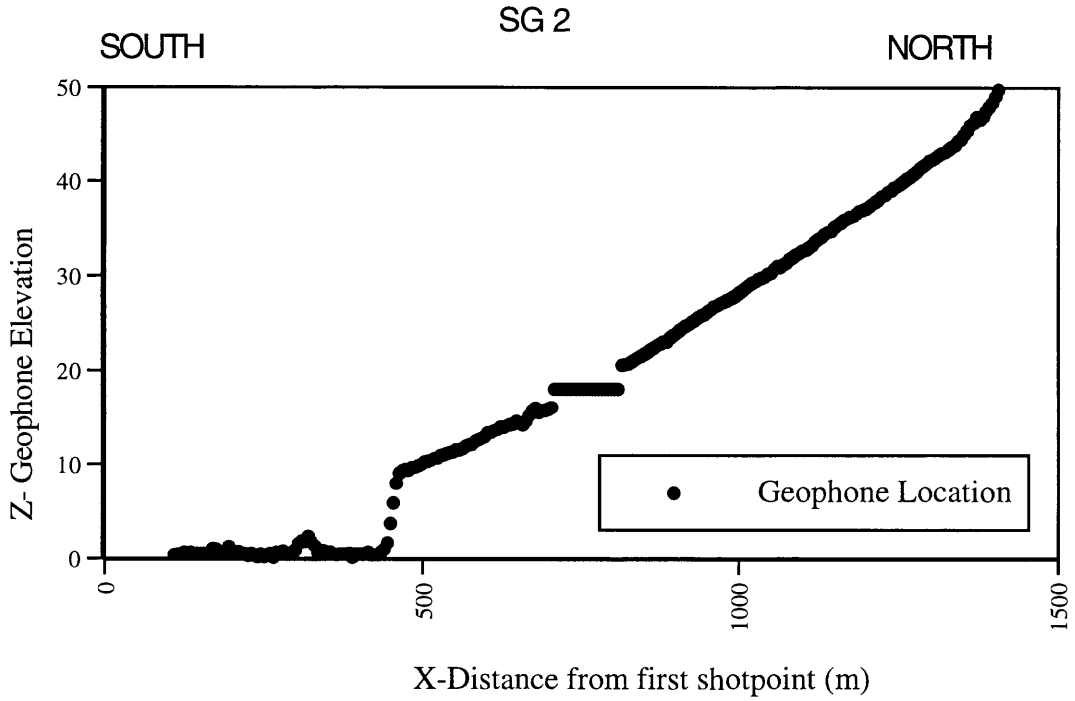

Figure 7. Geophone elevation in SG 2. Elevation is relative to the topographically lowest shot point.

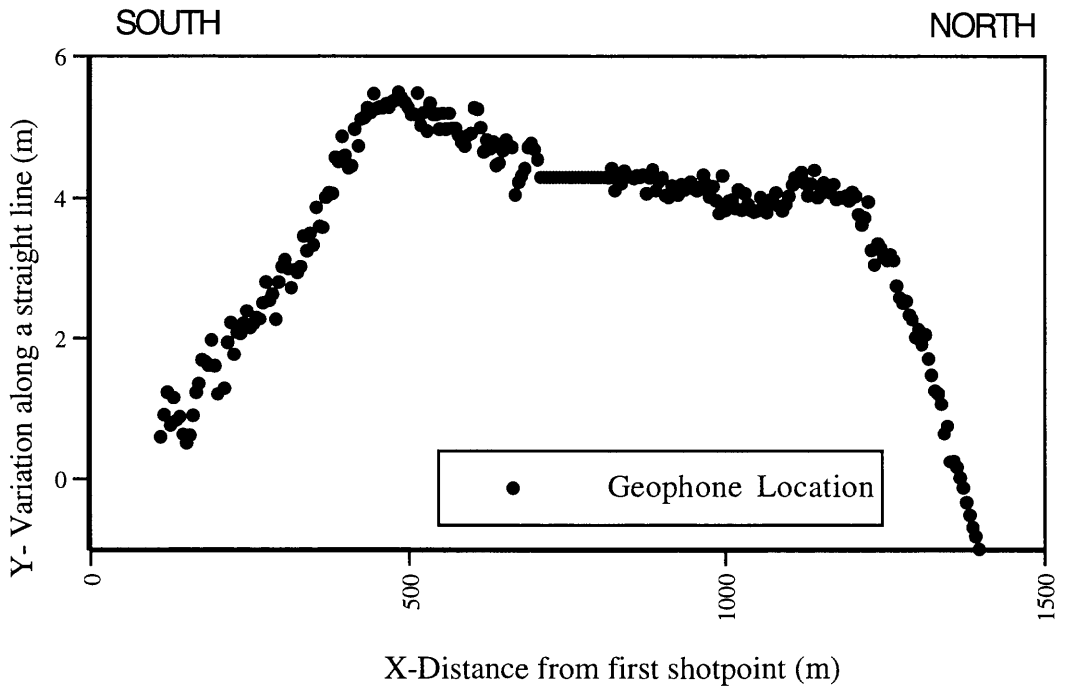

Figure 8. Geophone variation from a straight line connecting the first and last shot point south of the Colorado River Aqueduct.

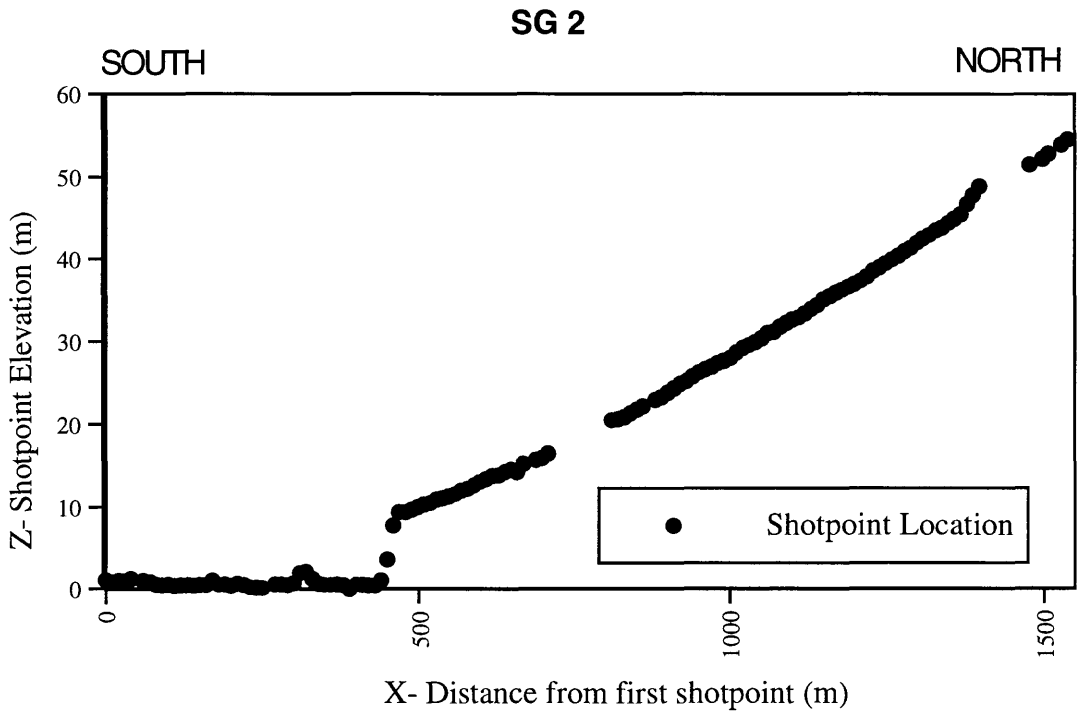

Figure 9. Shotpoint elevation along SG 2. Elevation is relative to the first shot point at the south end of the line.

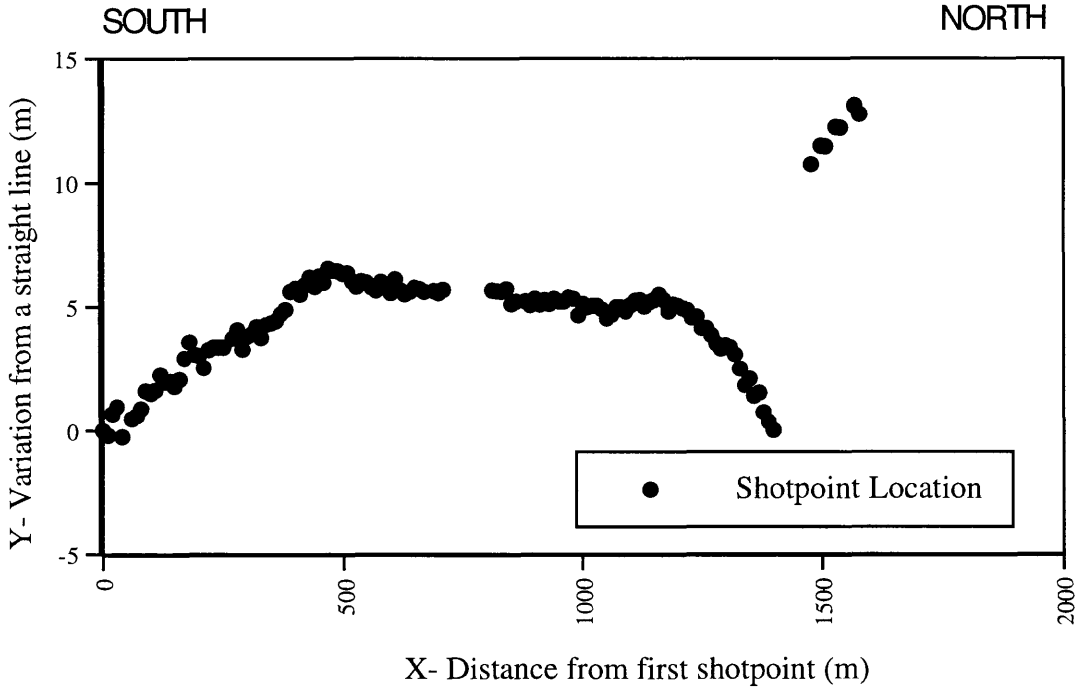

Figure 10. Shotpoint variation from a straight line connecting the first and last shotpoint south of the Colorado River Aqueduct.

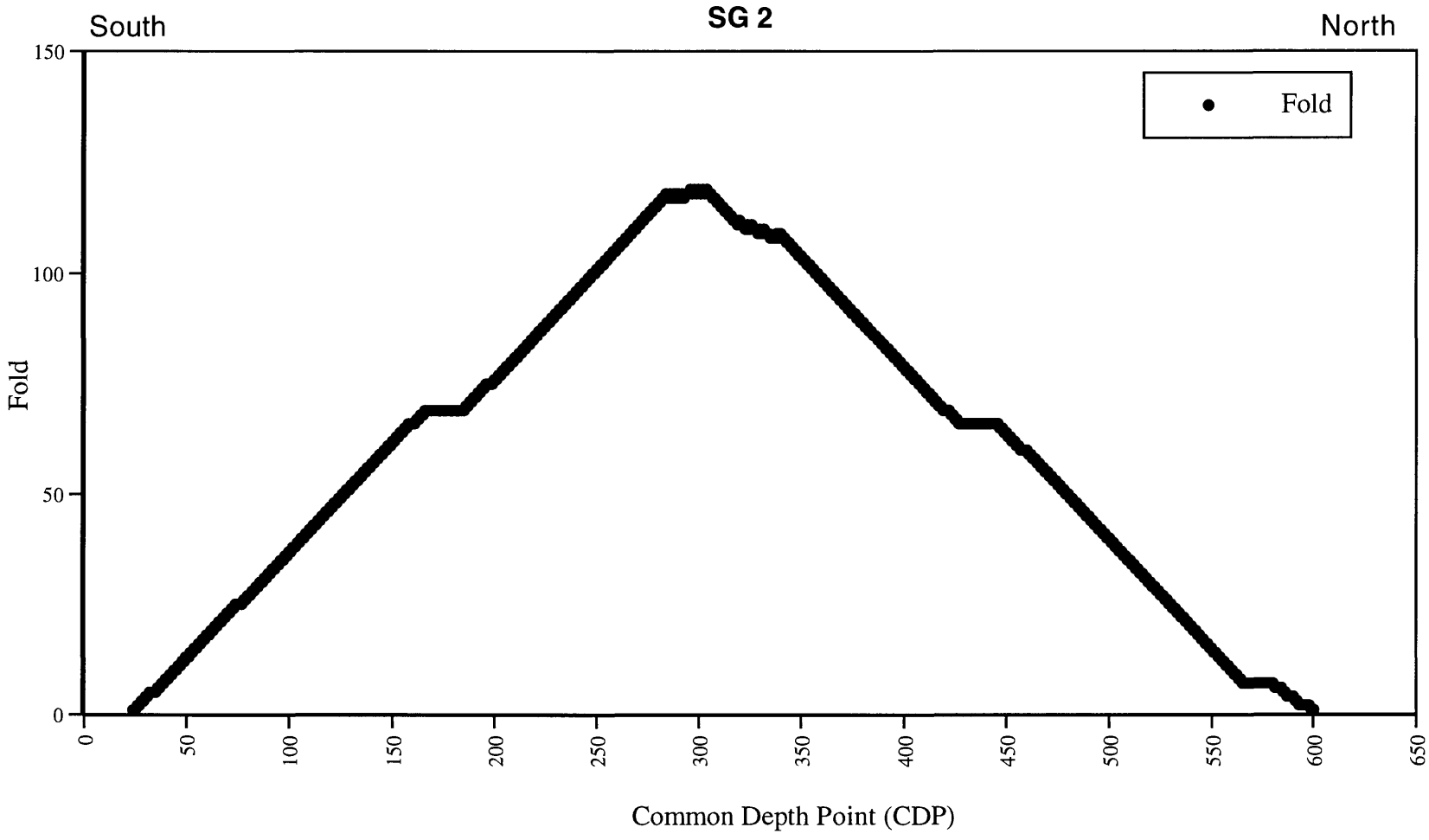

Figure 11. Fold as a function of common depth points along line SG 2. Distance is relative to first shotpoint at the south end of the line.

Interpretation

Profile SG 1

Interpreted Reflection Section

Migrated stacked seismic reflection images of the upper 1000 m (~3200 ft) along SG 1 are shown in figure 12. These data show numerous reflections from the near-surface to depths of approximately 1000 m, however, reflections beneath about 400 m depth are probably associated with reverberation of the seismic signal near the crystalline rock-sedimentary rock interface. Although there is lateral variation, in general, there are principal changes in the reflective character of the seismic section at depths of about 75 m and about 150-175 m, which are probably related to differences in lithology and/or physical properties of the subsurface at those depths. The seismic section above about 75 m probably corresponds to largely unconsolidated or poorly consolidated Quaternary sediments described by Allen (1957) (see Table 1). The lithology below the Quaternary sediments but above about 150 m depth is probably composed of Quaternary conglomerates, which Allen (1957) describes as ill-sorted conglomerates with clasts of crystalline rocks.

Interpreted Refraction Section

P-wave velocities range from about 800 m/s at the surface to about 3500 m/s at depths of about 225 m (Fig. 13). In the Cherry Valley area of the San Gorgonio Pass region, detailed seismic refraction measurements and well logs show that sediments with velocities of about 1500 m/s correspond to the depth of the static water level (Catchings et. al, 1999; Gandhok et al., 1999). Based on the well log for well MS-25 (Christensen, pers. comm), the lithology of the San Gorgonio Pass region (Allen, 1957), and the velocities observed in this survey, P-wave velocities below about 1500 m/s (at depths less than 200 m) are interpreted to represent unconsolidated and unsaturated Quaternary sediments. Velocities between about 1500 m/s and 3000 m/s in that depth range probably represent compacted or poorly consolidated sediments that may be saturated or unsaturated, depending on whether the predominant composition is sand or clay. Velocities in excess of 3000 m/s probably represent largely consolidated sediments (Mavko et al., 1996). Velocities representing fractured crystalline (metasedimentary) rocks of the San Gorgonio Pass region are likely to have velocities in excess of 4000 m/s, but our profile SG-1 was not long enough to obtain refractions from the depths needed to sample those velocities.

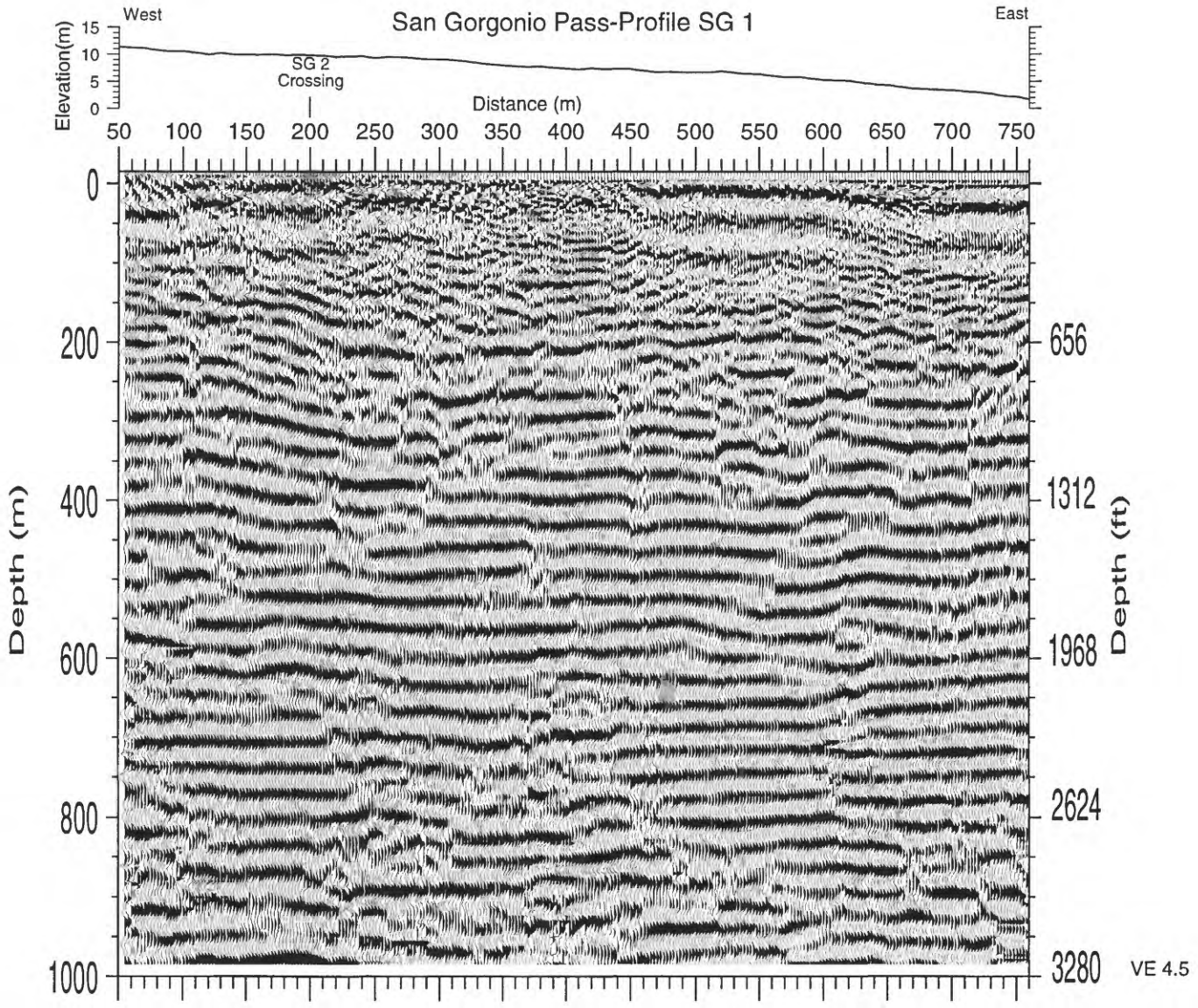

Fig. 12. Stacked and migrated seismic reflection section along profile SG 1.

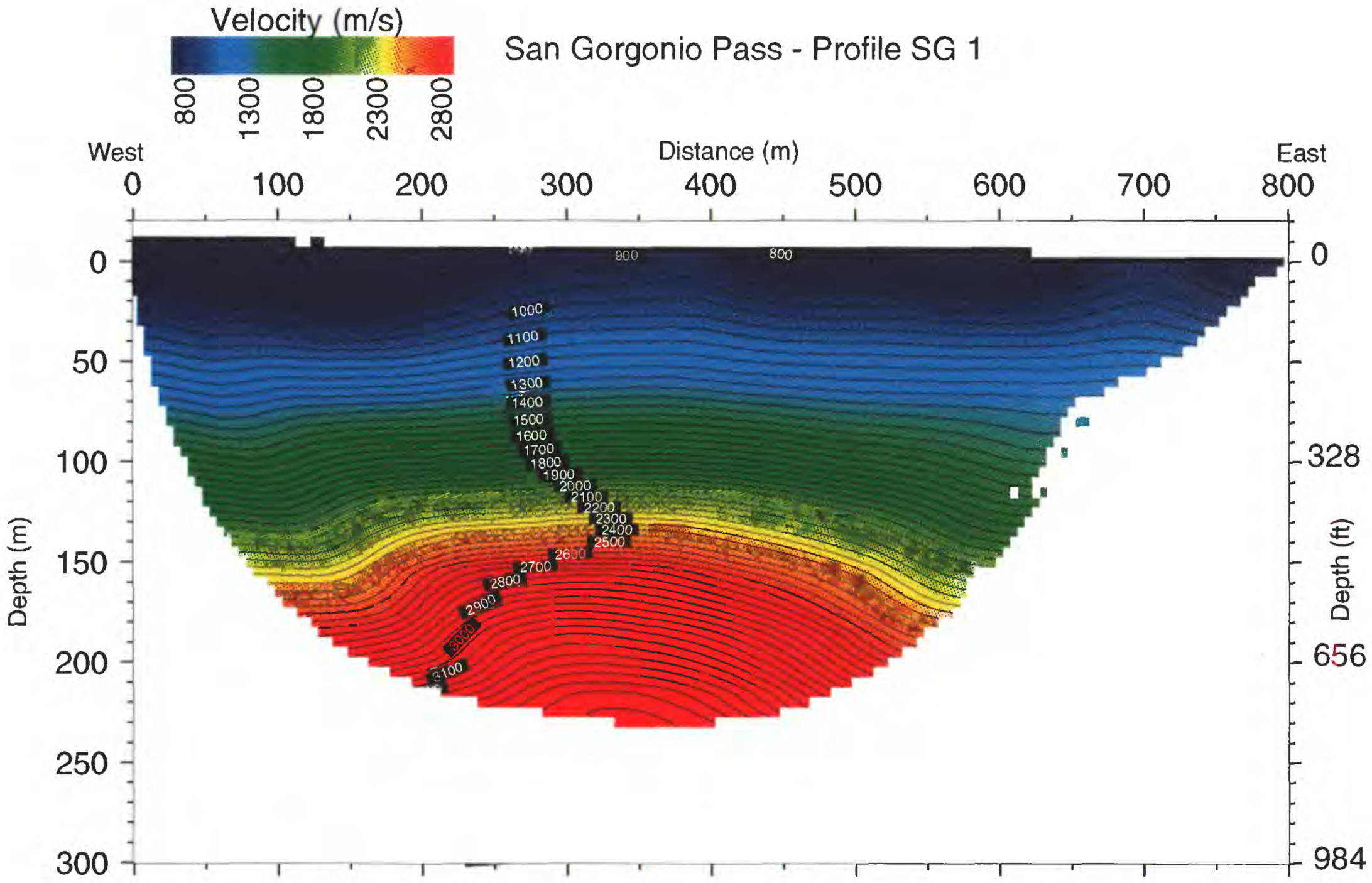

Fig. 13. Seismic refraction velocity inversion model along profile SG 1.

Interpreted Combined Refraction/Reflection

The combination of seismic velocities and seismic reflection images can be used to aid in interpreting the subsurface structure (Fig. 14a, 14b). Reflectors with velocities less than about 1500 m/s extend to about 85 m depth and probably represent largely unsaturated and unconsolidated sediments. This change in velocity coincides with a change in the reflection character, whereby, the reflectors apparently become more closely spaced. This depth range (below ground surface, bgs) is similar to that of the water level (82 to 86 m; 268 to 281 ft) observed in well MS-25 on August 29, 1997. Well MS-25 is located about meter 10 m north of meter 262 on profile SG 1. (Note: distances along the seismic profiles are referred to as meter "X", whereas depth is referred to as "X" m.)

A more irregular reflection pattern occurs from about 85 to 200 m depth, and velocities in that depth range are between about 1500 m/s and 3000 m/s. From about 85 m to about 200 m depth, the subsurface is probably dominated by saturated sediments (sands and clays) and poorly lithified rocks.

Reflections below about 200 m are more widely spaced and appear to become more reverbative with depth. Velocities in this depth range are between 3000 m/s and 4000 m/s. Subsurface rocks in this range probably represent partially lithified sedimentary rocks or clays. Below about 300 m depth, the reflections are highly reverberative. In numerous other seismic imaging investigations, we have found that the reflections become reverberative for depths below the sediment/hard-rock interface. The reverberative nature, combined with the high velocity (>3500 m/s) suggests that the rocks below about 300 m depth probably represent crystalline rocks, such as quartz monzonites observed in the San Bernardino Mountains to the north or metamorphic rocks observed to the south in the San Jacinto Mountains (Matti et al., 1992).

Generally, the pattern of reflections suggest that the unconsolidated and unsaturated sediments are thicker to the east, with maximum thickness approaching about 140 m. Although there are limited velocity data to the east, velocities are consistent with thicker sediments and deeper crystalline rocks to the east.

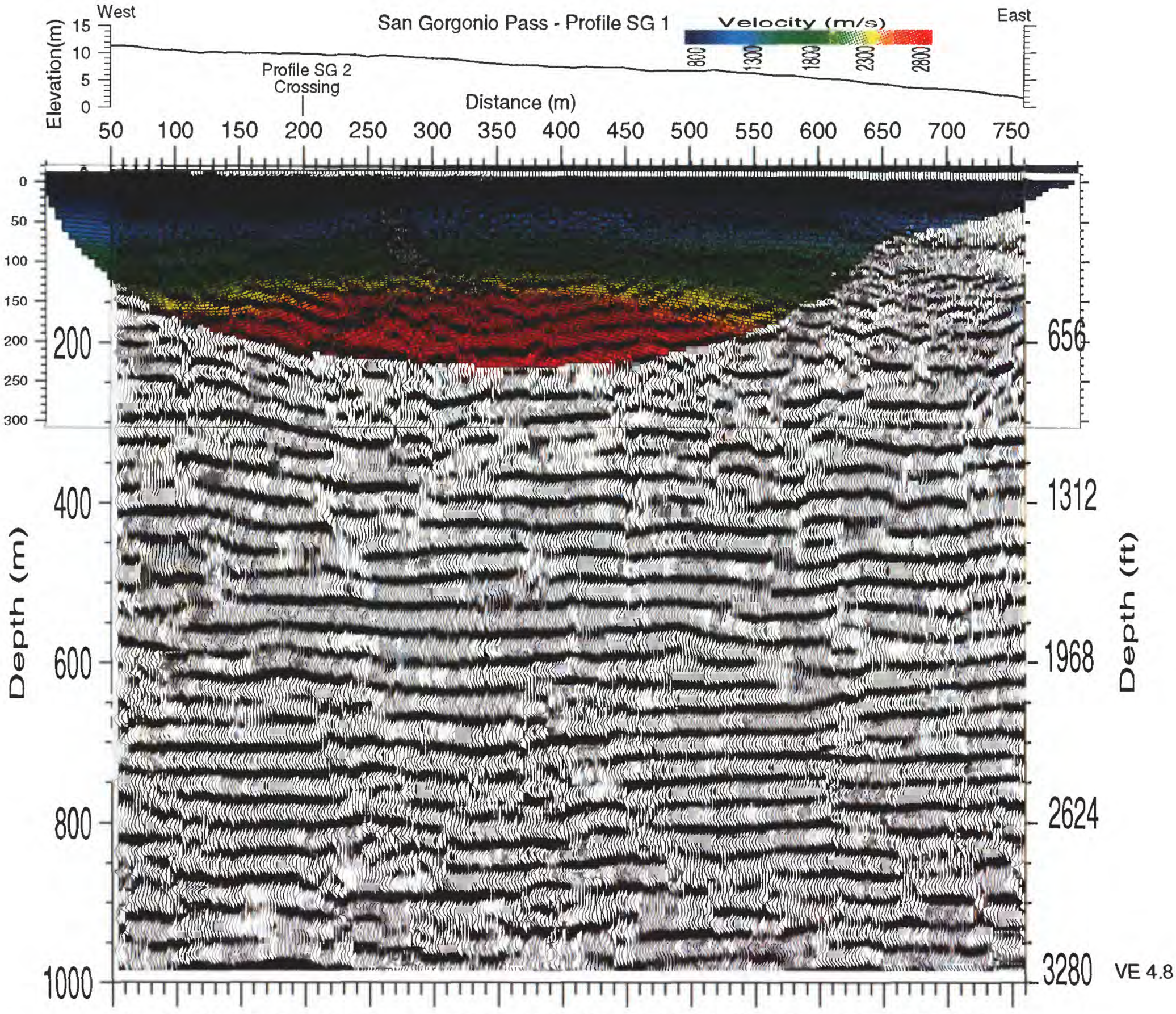

Fig. 14a. Combined seismic velocity model and migrated seismic reflection image along profile SG 1.

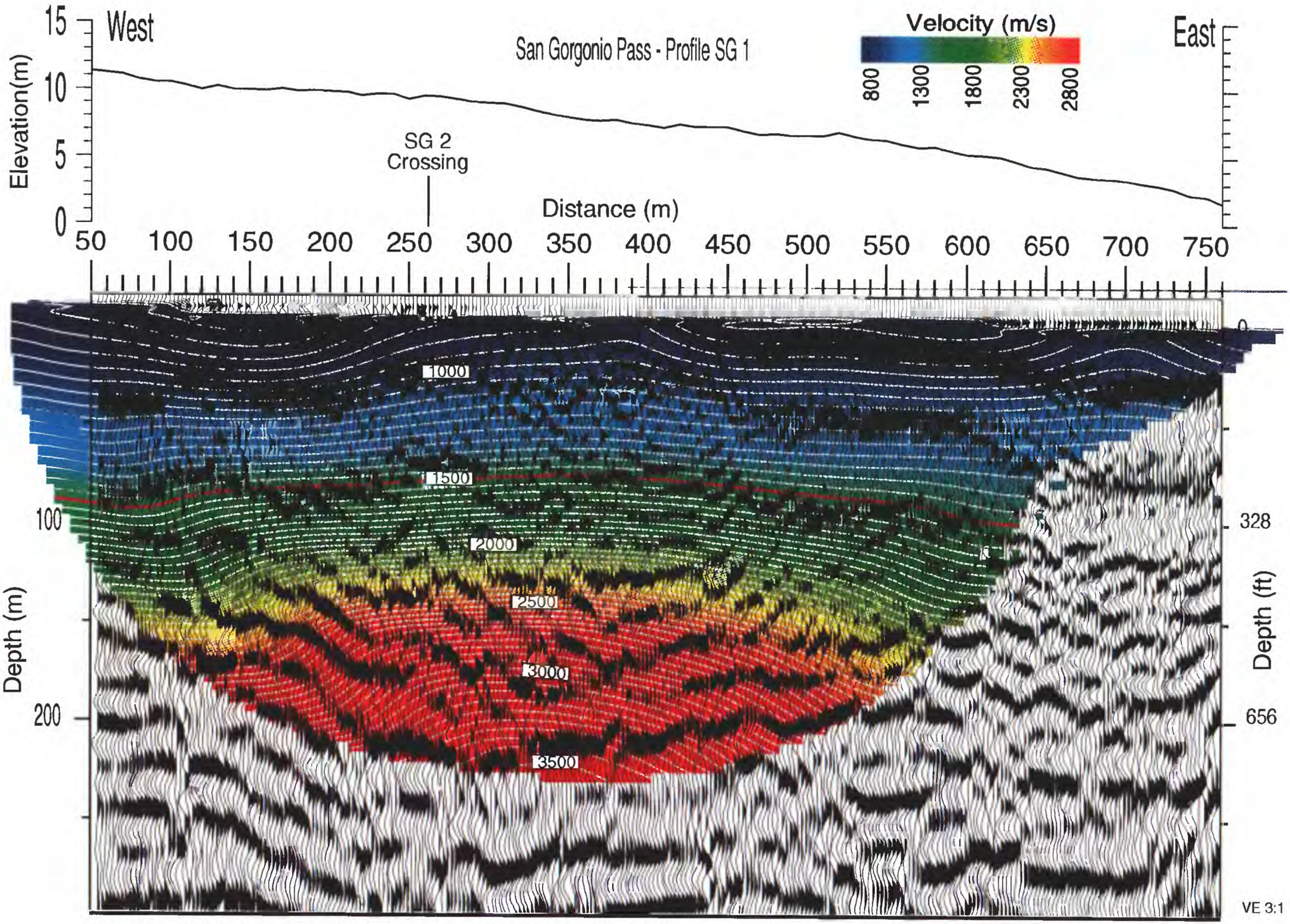

Fig. 14b. Seismic reflection and velocity inversion combined along profile SG 1. The 1500 m/s contour is shown in brown.

Profile SG 2

Interpreted Reflection Section

Unmigrated stacked seismic reflection images of the upper 1000 m (~3300 ft) along SG 2 are shown in figure 15. These data show numerous reflections from the near-surface to depths of approximately 300 m. Below about 300 m depth, the seismic section show strong reverberations that may result from reverberation of the seismic signal near the crystalline rock-sedimentary rock interface. There are large lateral variations in the seismic section from south to north. In the south, from about meters 0-450 distance, within the San Gorgonio River, the upper ~50 m (depth) of the subsurface is characterized by a well-layered, largely planar sequence of sediments. From about meters 500 to about meter 1000 distance, this sequence of sediments is thickest and less well layered. Northward of meter 1000, the well-layered sequence appears to thin and eventually pinch out.

In the depth range from about 50 to 100 m, the sedimentary sequence appears to be much less planar and irregular (Fig. 16). Abrupt offsets and diffracted sesimic energy suggest that the subsurface may be highly faulted at this depth. Higher-frequency diffractions are observed along most of the length of the profile below about 100 m depth. These high-frequency diffractions may arise from irregular surfaces such as large boulders or faults. A series of faults are apparent from the southern end of the profile to about meter 600; however, between meters 400 and 500, there appears to be an intense zone of faulting. This intense zone of faulting may be responsible for the strong, low-frequency apparent reflections from depths in excess of 300 m to about 1200 m in the distance ranges from about 550 m to about 1000 m. These apparent reflections suggest a northward dip of strata; however, due to the complexity of the structure observed and the number of diffractions observed on the section, it is likely that these apparent reflections do not represent the true structure. We used migration techniques to collapse diffractions and to move the reflected seismic energy to its proper location on the reflection section.

Migrated stacked seismic reflection sections of the upper 1000 m of profile SG 2 are shown in figure 16. The frequency content of the migrated section does not permit detailed resolution of the shallow sediments above 100 m depth, but structure below about 100 m is better characterized. These sections show that the strong, low-frequency, north-dipping reflections near the center of the seismic profile are actually south-dipping reflections that originate in the upper 300 m.

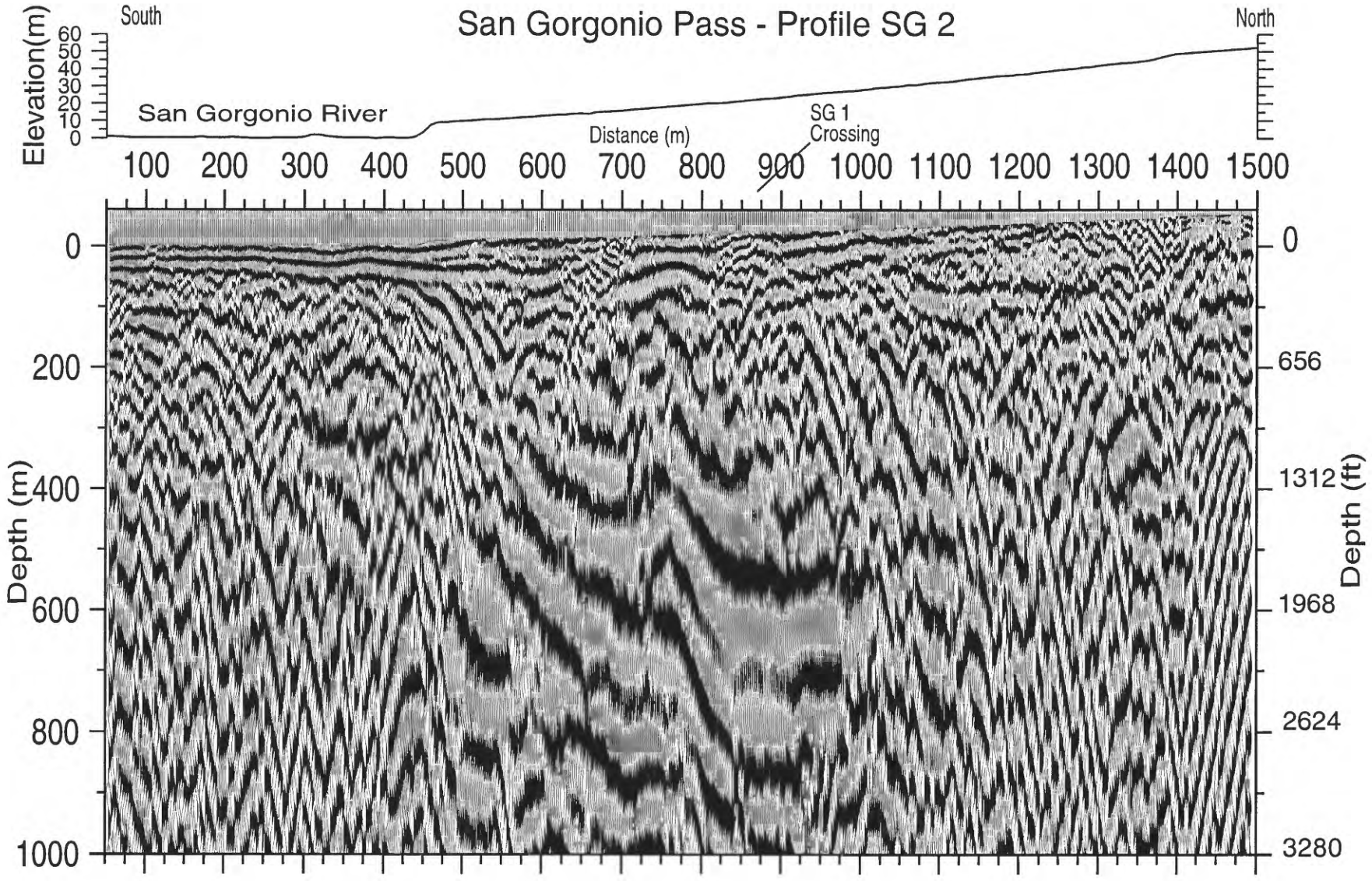

Fig. 15 Unmigrated stacked seismic reflection image along profile SG 2.

Processing Parameters
line 1r3 f1 a5 v2i: agc = 500, fk = 90-500, 15-200, 50%, bp = 15-30-100-200
poststack: bp = 1-5-20-40, agc = 50

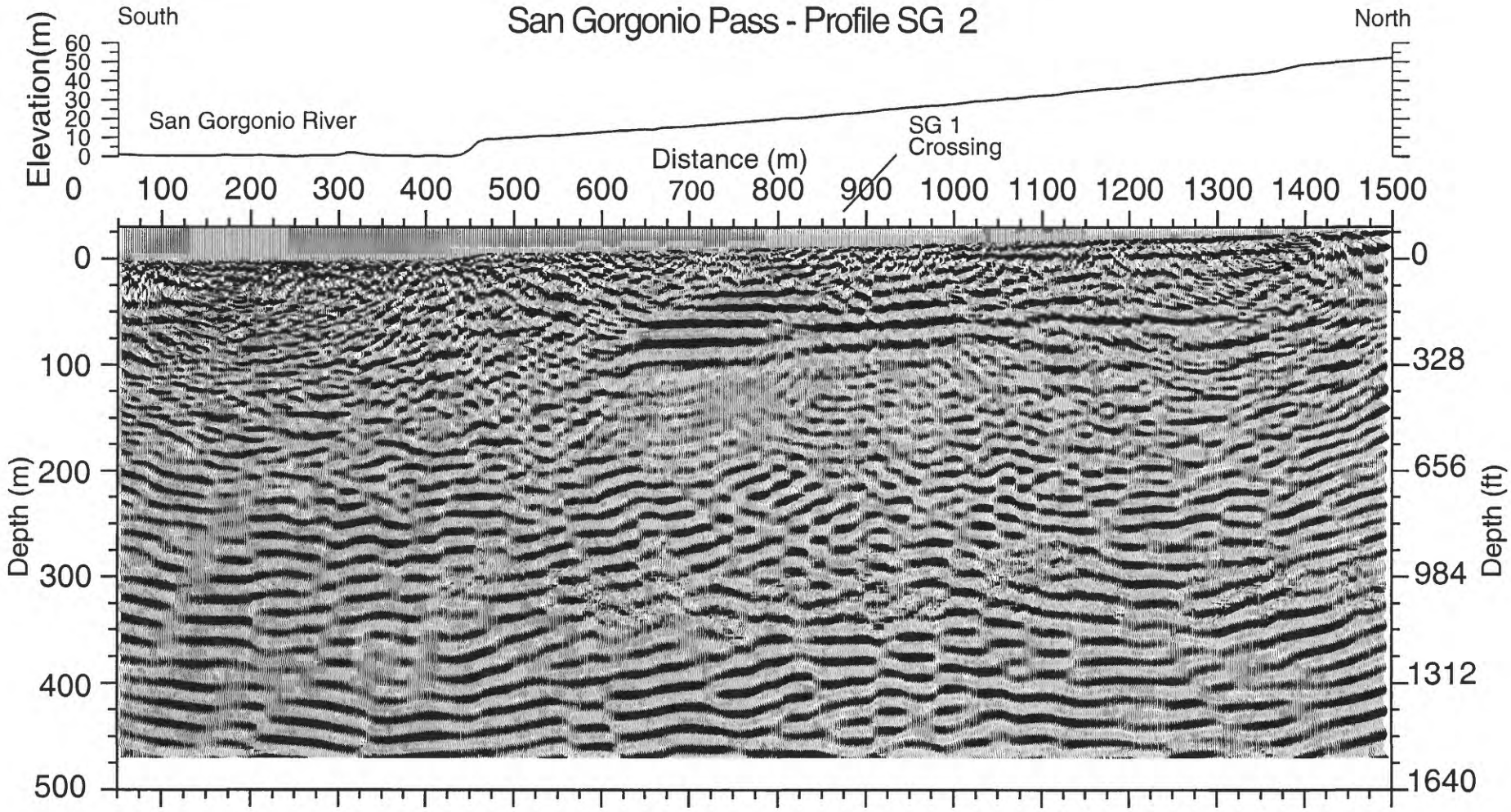

Fig. 16. Migrated seismic reflection image along profile SG 2.

Processing Parameters
line 1r3 k1 a5 p5 v2i: agc = 500, fk = 90-500, 15-200, 50%, bp = 15-30-100-200
mig = 100, 600, 90 poststack: bp = 15-30-600-1200, agc = 500

Interpreted Refraction Section

P-wave velocities range from about 700 m/s at the surface to about 4000 m/s at depths of about 350 m (Fig. 17). The velocities and interpretations are comparable to those described in the section on SG 1. Velocities that are less than 1500 m/s at depths of about 100 m likely represent unconsolidated and unsaturated Quaternary sediments. These sediments appear to be thicker in the southern part of the section. Velocities between the values of 3000 -4000 m/s probably represent consolidated rock (Mavko et al, 1996), and velocities greater than 4000 m/s likely represent consolidated rock.

Interpreted Combined Refraction/Reflection

The superposition of the velocity data on the reflection data for SG 2 also aids in interpreting the subsurface (Fig. 18a and 18b). The combined section shows that there is a general southward dip in structure toward the San Jacinto Mountains. The shallow, unconsolidated and unsaturated sediments are best seen on the unmigrated sections, but the velocity data show velocities less than about 1500 m/s that extend to depths of 85 m beneath meter 900 (where SG 1 crosses SG 2). These sediments apparently thicken to the south, where they are about 120 m thick at the southernmost end of the profile. The underlying, more consolidated sediments also dip to the south from the northern end of the profile to about meter 700. From about meter 700 to meter 0, the strata with velocities ranging from about 1500 m/s to about 3000 m/s appear to be folded and faulted in the upper 150 m and have northerly as well as southerly dips (Fig. 18b). The thickness of this strata increases from about 150 m at meter 900 to nearly 250 m toward the southern end of the profile. Crystalline rocks (>4000 m/s) also deepen from the north to the south.

Discussion and Conclusions

Stratigraphic Horizons:

One of the principal objectives of this study was to map the basic stratigraphic horizons, including the depth to the base of the unconsolidated sediments and the depth to the top of crystalline rock. If the stratigraphic depths were known in a particular location from well logs, the seismic images and velocities could be used to laterally map the stratigraphy based on correlation with the well logs. However, the only well in the immediate vicinity of the seismic profiles was Well MS-25, which at 142 m (465 ft) depth did not reach crystalline rock and may not have reached the base of the unconsolidated sediments. The well log, described as "sand, gravel, and boulders to a depth of 465 ft" did not provide much detail about the stratigraphy. Although the stratigraphy is not well

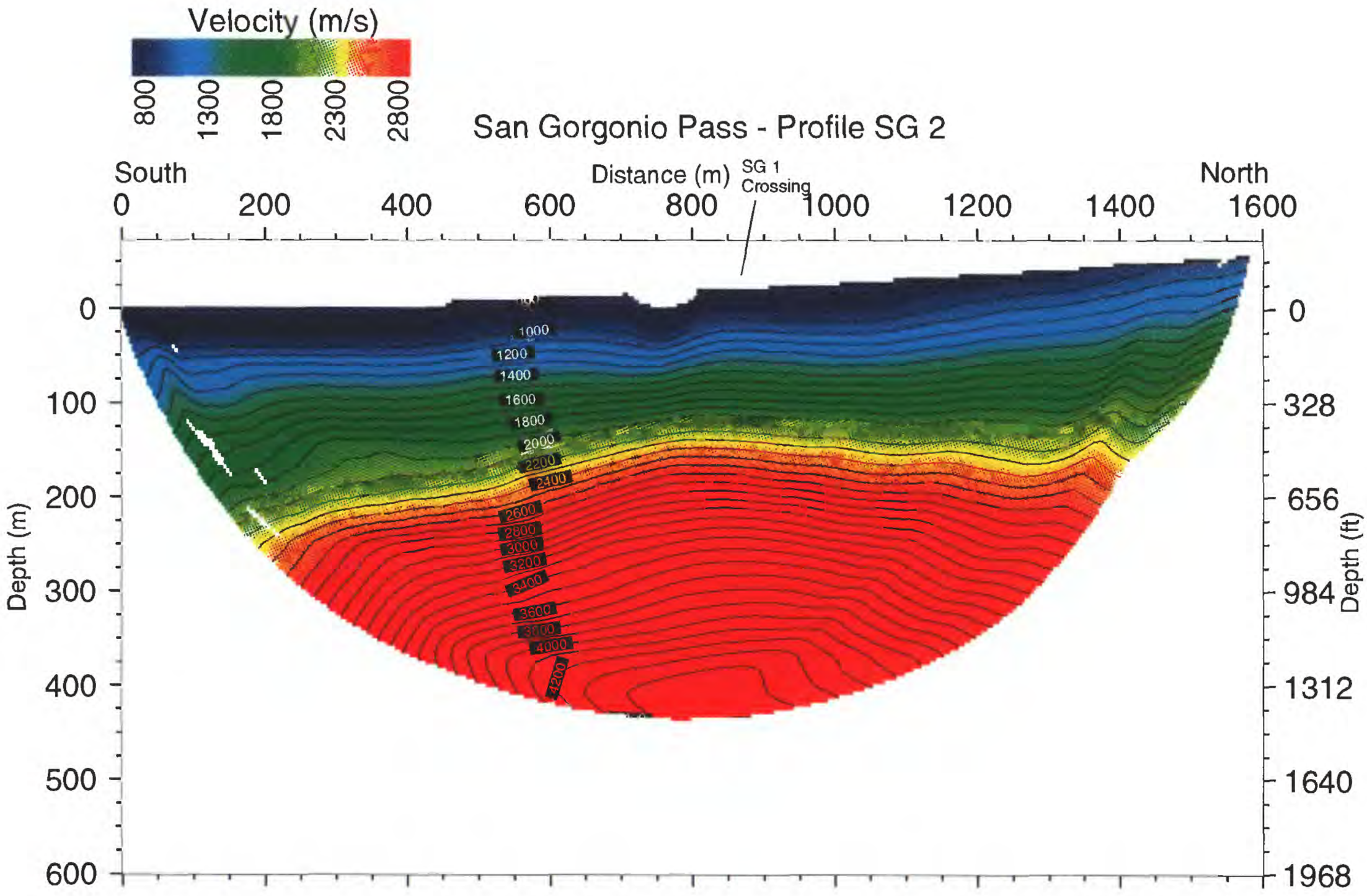

Fig. 17. Seismic refraction velocity inversion model along profile SG 2.

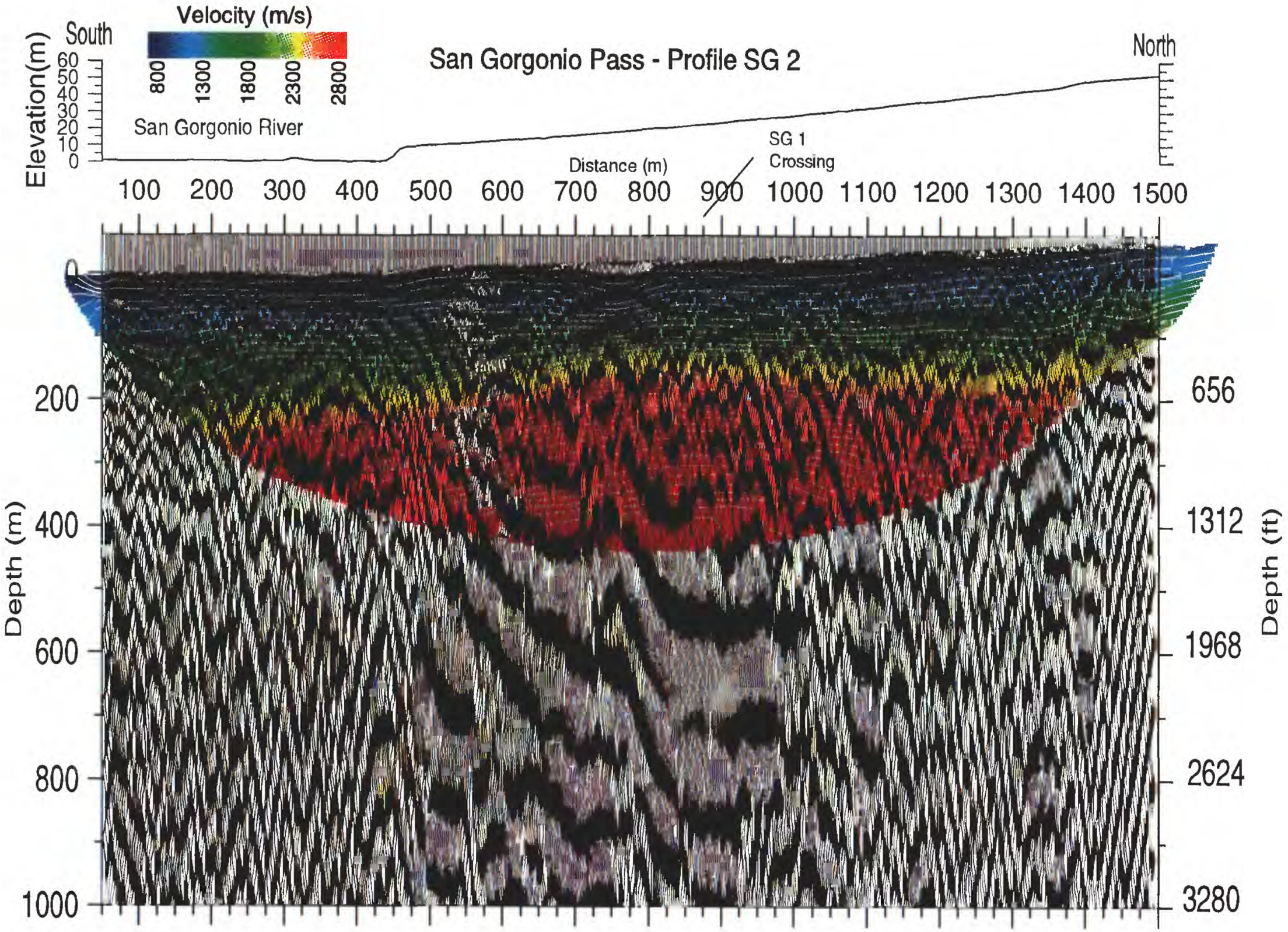

Fig. 18a. Combined seismic velocity and unmigrated seismic reflection image along proifle SG 2.

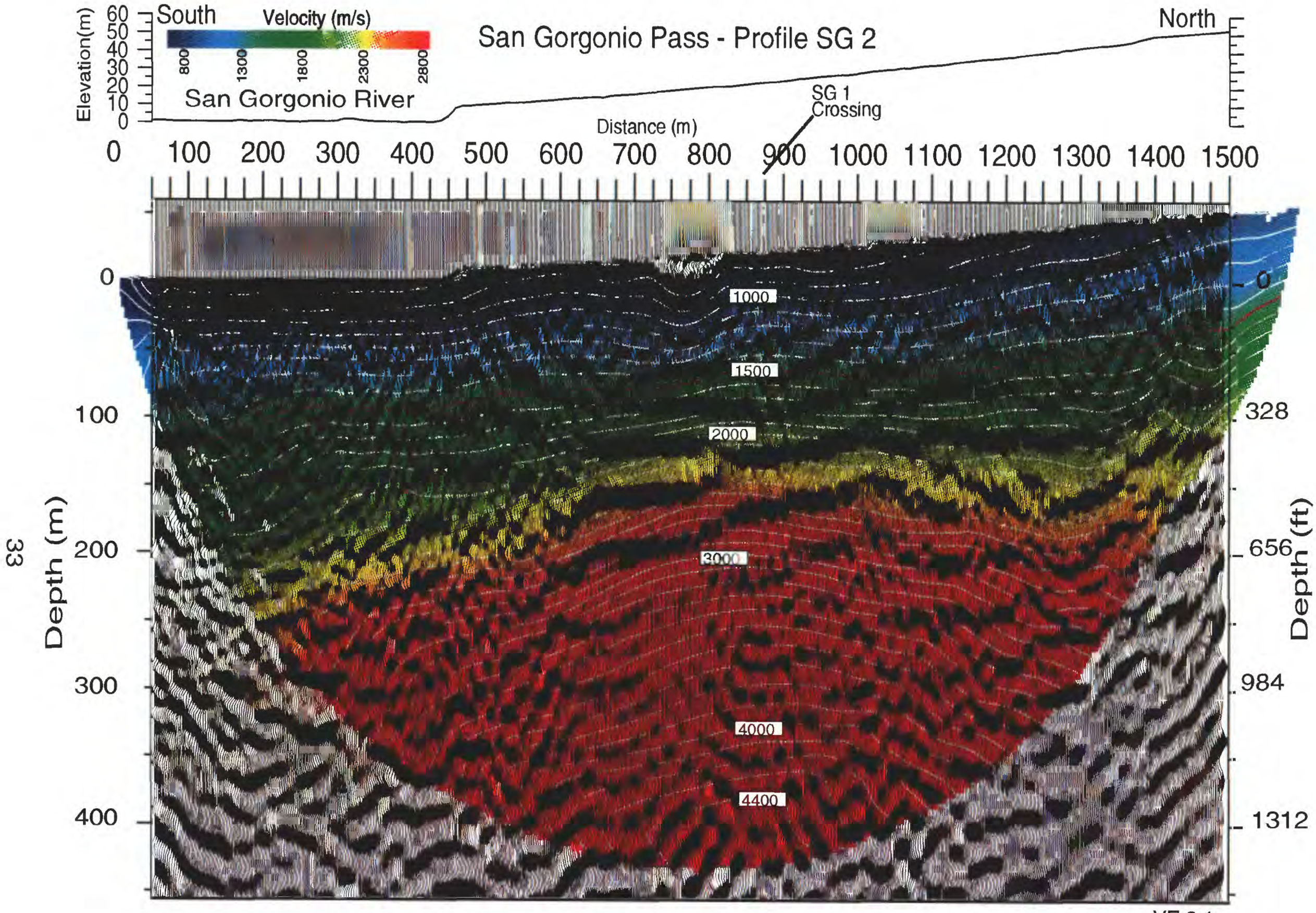

Fig. 18b Combnined seismic reflection image and velocity inversion model along profile SG 2. Brown line denotes 1500 m/s contour.

determined from the MS-25 well-log, that well log, combined with seismic velocity and seismic reflection images, can be used to provide considerable constraints on the stratigraphy. A number of factors other than composition can influence the seismic velocity of subsurface strata, including depth of burial (pressure), how well lithified the sediments are, degree of water saturation, degree of faulting and fracturing, etc., but most lithified sedimentary rocks are likely to have compressional velocities (Vp) greater than about 2500 m/s. For example, from laboratory experiments, Nur (1982) shows Berea and Massilon sandstones (both highly porous sandstones) have miminum compressional velocities of about 3100 m/s and 2800 m/s, respectively, at 0 effective pressure (atmospheric pressure = pressure at the surface). These rocks have much higher velocities at higher pressures (greater burial depths), but if we adopt the minimum velocity of 2800 m/s as the velocity of lithified sediments in San Gorgonio Pass, the minimum depth of lithified sediments (Vp=2800 m/s) would range from about 160 m to more than 200 m along profile SG 1 (Fig. 13). Considering both the velocity data and the reflection data, it is likely that a strong reflection and a change in the reflection pattern at about 200 m depth represent the base of unconsolidated sediments and the top of consolidated sediments (Vp = 3300 m/s). Along profile SG 2, the depth to the 2800 m/s contour is greater than about 250 m, suggesting that unconsolidated sediments extend to that depth near the northern end of the San Jacinto mountains. These unconsolidated sediments appear to thin to about 200 m total thickness beneath the I-10 freeway, but appear to thicken to about 280 m near the north end of the profile. The apparent thickening to the north and south may be due to a increased sedimentation near each mountain range.

For both Berea and Massilon sandstones, velocities at pressures of up to 800 bars (depths of ~2 km) are about 4100 m/s and 3800 m/s, respectively (Nur, 1982). For the ill-sorted conglomerates and sandstones that should underly San Gorgonio Pass at shallower depths (Allen, 1957), we should expect similar velocities. If we assume the ~4000 m/s velocity to approximate the base to the consolidated sedimentary rocks, then the mimimum depth to crystalline basement rocks should be at about 350 m along profile SG 2, increasing to the south. A change in the reflection pattern, even though it is reverberative, also occurs at this depth near the center of the profile.

Water Level

Because the velocity of seismic compressional waves in water is approximately 1500 m/s, and the velocity of compressional waves in unconsolidated sediments is approximately the same (Schon, 1996), we can use the detailed velocity measurements to laterally map the water level along profiles SG1 and SG 2. The depth to the water level in

Well MS-25 (located at about meter 262 on SG 1 and meter 875 on SG 2) was determined to be between 82 m (268 ft) and 86 m (281 ft) on August 29, 1997. The 1500 m/s velocity contour on both profiles near Well MS-25 is about 85 m, consistent with the depth found in the well. Toward the southern end of profile SG 2, near the San Jacinto mountains, the 1500 m/s contour (and presumably the water level) increases in depth to about 115 m to 120 m. Near the very ends of the seismic profiles, the velocity contours may experience edge effects, but near the northern end of profile SG 2, the depth to the water level apparently decreases to about 75 m. Along profile SG 1, the apparent water level (1500 m/s contour) appears to increase slightly (to about 90 m depth) to the east (at meter 600), but we do not have velocity data near the eastern end of the profile at the depths needed to map the 1500 m/s coutour. In general, the water table appears not to vary greatly (~5 m) from east to west along the profiles, but it does vary appreciably (~30 m) from north to south.

Faults:

Faulting in the San Gorgonio Pass region is known to be highly complex (Matti et al., 1992), and our interpretation of faulting (Figs. 19 and 20) on the seismic sections is consistent with the complexities observed by surface mapping (Matti et al., 1992). Along profile SG 1, there appear to be smaller near-vertical faults along much of the section and more pronounced faults appear to be located toward the eastern end of the profile, surfacing near meters 610 and 690 (Fig. 19). Along much of the profile, the cummulative effect of the smaller faults appears to have vertically offset layers in the upper 100 m by as much as 25 m. Near the central and western end of SG 1, there appear to be a series of apparent small horst and graben structures, with each horst or graben being less than about 100 m wide. Near the western end of profile SG 1, there appear to be minor folding of strata between 100 m and 300 m depth, with the apex of the fold to the west. Due to its limited length and apparent semi-parrallelism with regional fault systems, faulting and folding relationships are difficult to understand along profile SG 1 and will have to be combined with surface mapping and other seismic investigations to fully understand them.

Profile SG 2 trends largely perpendicular to the regional fault systems and is about twice the length of profile SG 1, allowing better images of apparent faults and folds (Fig. 20). In the northern half of profile SG 2, there appear to be several high-angle (~65° to 70°), north-dipping faults that may have offset strata by less than about 10 to 20 m. Toward the center of the profile, however, high-angle faults appear to be south-dipping along the north limb of an apparent fold. There appear to be two folds in the upper 100 m along the southern half of profile SG 2 that seem to be related to one or more north-dipping thrust faults. These apparent thrust faults appear to surface south of the southern end of

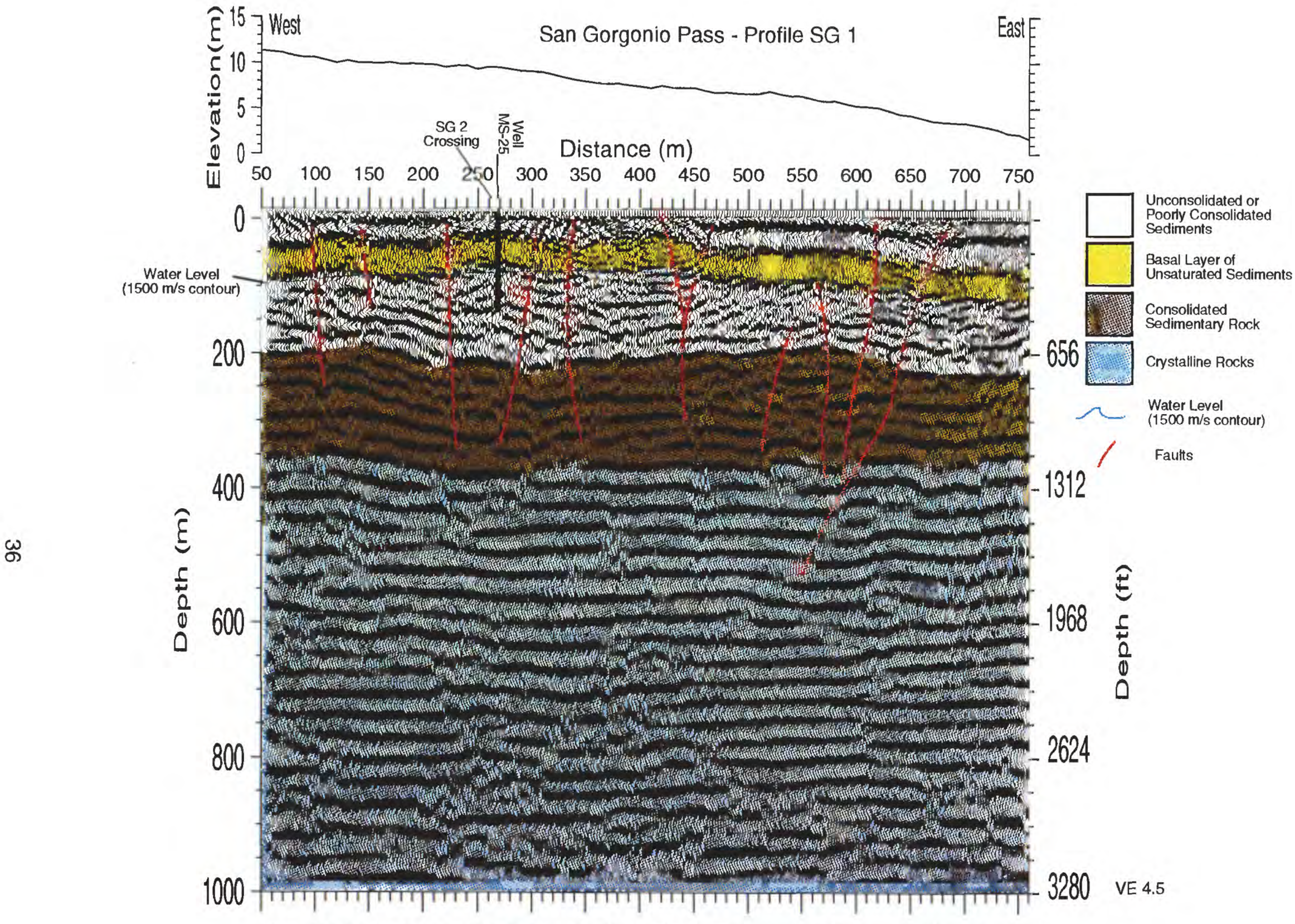

Fig. 19. Interpreted seismic image along SG 1. The depth of the water Level, which correlates with the 1500 m/s contour from the velocity model (Fig. 13), is determined from Well MS-25.

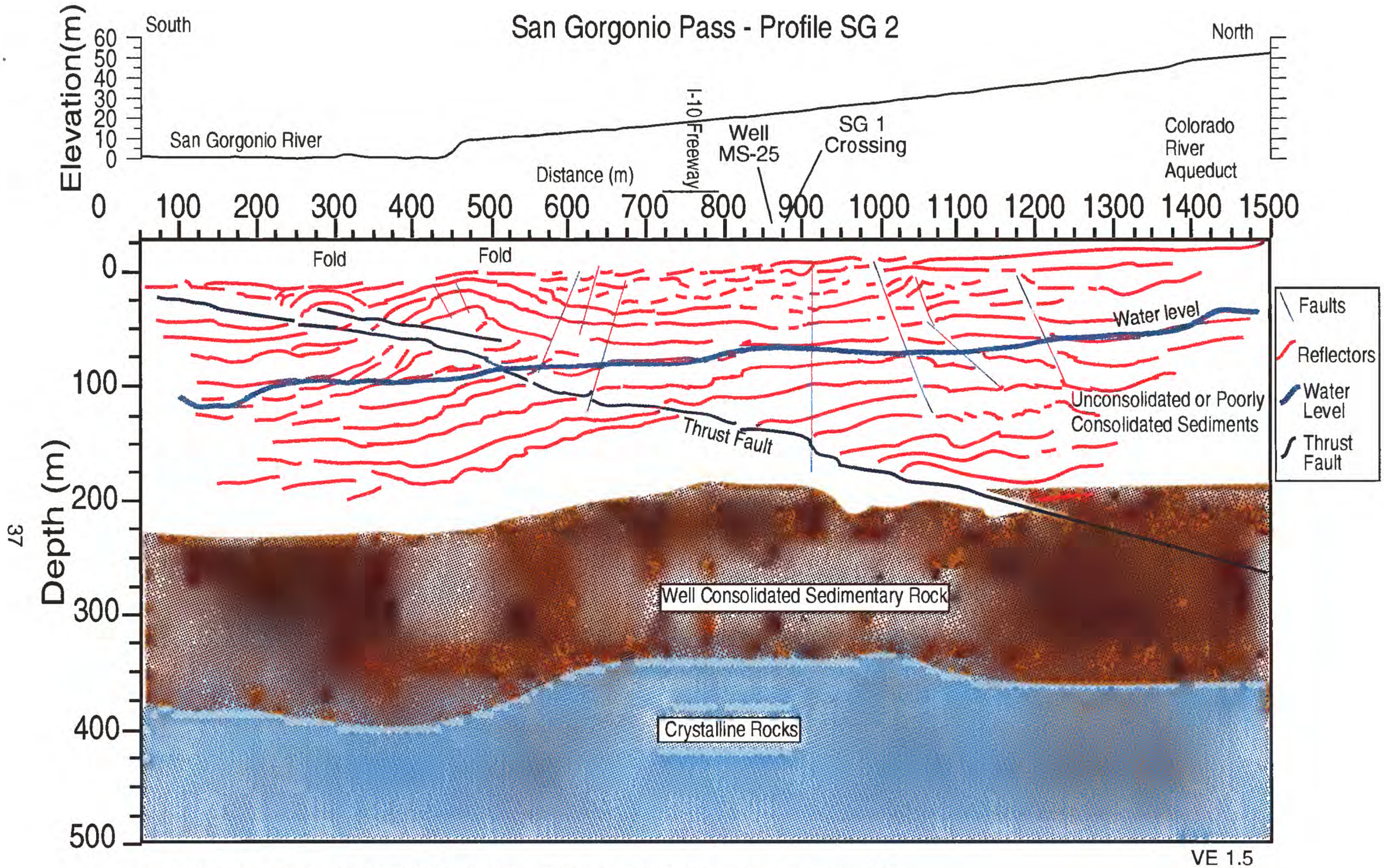

Fig. 20 Line drawing and interpretation of seismic reflection and refraction data along profile SG 2.

profile SG 2 and dip northward between 10° and 15° across profile SG 2 in the upper few hundred meters. As interpreted, the apparent thrust fault is located within the unconsolidated sediments and sedimentary rocks (above crystalline basement) along the entire profile.

We acknowledge that the apparent folds and faults along profile SG 2 can be interpreted differently, but we have chosen this interpretation because it appears to fit the seismic image and it explains other observations in the data. For example, a north-dipping thrust fault better explains the presence of low-frequency, north-dipping reflectors that are observed on the unmigrated seismic sections (between 200 m and 1000 m depth) near the center of profile SG 2, and the folds account for the north- and south-dipping reflections above 200 m depth on the southern half of the profile SG 2 (Fig. 15). Furthermore, the velocity model for profile SG 2 shows that velocities greater than about 2500 m/s increase in dip southward near the center of the seismic profile which is consistent with the expectation of thicker sediments as a result of thrusting to the south.

Implication for Water Resources:

The seismic data suggests that the upper 200 m of the subsurface along profile SG 1 consists largely of unconsolidated sediments. The water level (1500 m/s) appears to range from about 85 m to 90 m below the ground surface, with a slight increase in depth to the east (Fig. 14b). There is apparent faulting along most of the seismic profile (Fig. 19), but the smaller faults do not appear to affect the depth of the 1500 m/s contour (water level). However, because the velocity model has been laterally and vertically smoothed (5-m smoothing), the 1500-m/s contour may not accurately reflect small changes in the depth to the water level. If the reflection that correlates with the 1500-m/s contour arises from the water table (Fig. 14b), then this reflection suggests that the water table rises and deepens laterally across the faults by several meters. However, the more prominent faults near the eastern end of the array suggests that the water table is affected by faults to a greater extent, as the water table (1500 m/s contour and reflector) appears to deepen to the east.

The predominant water-bearing strata is probably between about 85 m and 200 m depth because velocities beneath 200 m depth are sufficiently high that it is unlikely that the rocks are porous at that depth. It is possible that these rocks are highly fractured, which in theory, could significantly increase the secondary permeability. However, cements in non crystalline (sedimentary) rocks typically limit the fracture permeability, suggesting that they are probably not very permeable below about 200 m depth. The seismic data suggest that the water-bearing strata is probably from about (relative to ground surface) 120 m to about 250 m deep (~130 m thick) near the southern end of profile SG 2 and is about 75 m to

about 250 m deep (~175 m thick) near the northern end. The depth to the top of the water level appears to decrease slightly to the south across the apparent thrust fault.

These observations suggest that the water table varies laterally in both east-west and north-south directions, with the greatest variation from north to south. The lateral variations are due to large-scale structure, such as basin structure, and to smaller scale structures, such as faults. Lateral flow across faults is probably inhibited by the structure of the faults, an important consideration with respect to groundwater flow modeling and water storage.

Correlations with existing well data, along these profiles and at other locations within San Gorgonio Pass, indicate that these seismic methods are ideal for mapping the water table and its lateral variations.

Implications for Earthquake Hazards:

The seismic data, combined with exisiting surface mapping (Matti et al., 1992) suggest that San Gorgonio Pass is underlain by numerous high-angle (> 60°) faults and more than one low-angle (~15° to 20°) thrust faults at shallow depths. The lateral extent of the imaged thrust faults are not known, but if the imaged fault is comparable to the mapped thrust faults to the north, the imaged fault is probably laterally connected to other thrust faults by high-angle faults. To the north, the imaged fault may also be connected to the mapped fault at depth, whereby both sole into one fault. The presence of such faults across most of the valley within San Gorgonio Pass, suggests that the hazards to the Pass, its infrastructure, and to through-going lifelines are greater than those from a single fault system located on the northern end of the Pass.

Because of the large number of seismic events recorded beneath, north, and south of San Gorgonio Pass between 1981 and 1993 (Magistrale and Sanders, 1996) and due to the presence of the regional lifelines trending through the Pass, it is clear that there is a considerable seismic risk within San Gorgonio Pass. Shaking induced by movement on local faults, such as those observed in the present seismic survey, or on the regional faults (San Andreas or San Jacinto) will likely be amplified by the thick (up to 200 m) accumulation of low-velocity sediments that underlie most of San Gorgonio Pass.

Matti et al. (1992) suggest that surface faulting younger than about 2800 years has not yet been identified in the central San Gorgonio Pass region, but the seismic data from this study suggests that faults in the San Gorgonio River may propogate to the very near (within 3 meters or less) surface. Because of the flooding history in the area, it is likely that the faults identified in the seismic sections at only 3 m depth are relatively young.

Trenching studies should be utilized within the San Gorgonio River to help date the apparent faults.

Future seismic risk assessments and hazard analyses should incorporate the results of the present study and more comprehensive investigations, utilizing a wide array of geological, geophysical, and hydrological methods, should be considered for the San Gorgonio Pass region to improve water-resource management and to mitigate hazards.

Data Availability

The data are available as shot gathers with elevation and timing corrections applied in SEG-Y format from R.D. Catchings at the address in the front of this report.

Acknowledgements

We thank Jeff Dingler, Jamie Fenimore, Joseph Grow, Monique Jaasma, Gernot Lagand, Nicole Lautze, Janice Murphy, Keith Rice, Jose Rodriguez, and Marjan Rotting for assistance in acquiring the seismic data. The project was funded by the Morongo Indian Reservation and the U. S. Geological Survey.

References

Allen, C.R., 1957,San Andreas fault zone in San Gorgonio Pass, southern California: Geological Society of America Bulletin, v. 68, p. 319-350.

Catchings, R. D., E. Horta, M. R. Goldman, M. J. Rymer, and T. R. Burdette, 1998, High-resolution seismic imaging for environmental and earthquake hazards assessment at the Raychem Site, Menlo Park, California, U. S. Geol. Surv. Open-File Report 98-146, 37 pp.

Catchings, R. D., M. R. Goldman, W. H. K. Lee, M. J. Rymer and D. J. Ponti, 1998, Faulting Apparently Related to the 1994 Northridge, California, Earthquake and Possible Co-Seismic Origin of Surface Cracks in Potrero Canyon, Los Angeles County, California, Bull. Seism. Soc. Am. v.88,1379-1391.

Catchings, R.D., G. Gandhok, M.R. Goldman, E. Horta, M.J. Rymer, P. Martin, and A. Christensen, 1999, High-resolution seismic reflection/refraction imaging beneath Cherry Valley, Riverside County, California: Implications for water resources and earthquake hazards, U.S. Geol. Surv. Open-File Report 99-26, 60 pp.

Christensen, N. I. (1996). Poisson's ratio and crustal seismology, J. Geophys. Res. 101, 3139-3156.

Gandhok, G., R. D. Catchings, M.R. Goldman, E. Horta, M.J. Rymer, P. Martin, and A. Christensen, 1999, High-resolution seismic reflection/refraction imaging from I-10 to Cherry Valley Blvd., Cherry Valley, Riverside County, California: Implications for water resources and earthquake hazards, U.S. Geol. Surv. Open-File Report 99-320, 52 pp.

Fumal, T. E., J. F. Gibbs, and E. F. Roth 1981, In-situ measurements of seismic velocity at 19 locations in the Los Angeles, California region, U.S. Geol. surv. Open-File Rept. 81-399, 119 pp.

Fraser, D.M., 1931, Geology of the San Jacinto quadrangle south of San Gorgonio Pass: Calif. Div. Mines 27th Rept. of State Mineralogist, p.494-540.

Hole, J.A, 1992, Nonlinear high-resolution three-dimensional seismic travel time tomography, J. Geophys. Res., v. 97, p. 6553-6562.

Magistrale, H. M., and C. Sanders, 1996, Evidence from precise earthquake hypocenters for segmentation of the San Andreas fault in San Gorgonio Pass, J. Geophys. Res., v. 101, 3031-3044.

Matti, J.C., D.M. Morton, B.F. Cox, 1992, Distribution and geologic relations of fault systems in the vicinity of the central Transverse Ranges, Southern California, Open-File Report 92-354.

Matti, J.C., and D.M. Morton, 1982, Geologic history of the Banning fault zone, southern California: Geological Society of America Abstracts with Programs,v.14, no.4,p. 184.

Mavko, G., T. Mukerji, and J. Dvorkin, 1996, Rock Physics Handbook, Stanford Rock physics Laboratory, Stanford University, Stanford, California, 323 pp.

Nur, Amos, 1982, Notes on wave propagation in porous rocks, Stanford Rock Physics Project vol. 13, Stanford, California, 121 pp.

Schon, J. H., 1996, Physical properties of rocks: Fundamentals and principles of petrophysics, Handbook of Geophysical Exploration (Seismic Exploration), v. 18, Pergamon Press, Elsevier Science, Inc., Tarrytown, New York, 583 pp.

Appendix A

Distances and elevations along SG 1 seismic line.
Measurements are relative to first shotpoint at the west end of the line.

Geophone Sta #	Receiver Dist (m)	Receiver Elev. (m)	Shot Sta. #	Shot Distance (m)	Shot Elev. (m)
			1	0	11.67
			3	10.22	11.75
			5	19.6	11.94
			7	30.37	11.59
			9	40.09	11.42
			13	50.32	11.31
			15	60.21	11.2
			17	69.78	11.06
			19	80.32	10.71
			21	90.13	10.51
			23	100.01	10.49
1	110.21	10.25	25	109.59	10.26
2	115.11	10.09			
3	120.2	10	27	119.98	9.92
4	125.16	10.12			
5	130.24	10.19	29	129.97	10.17
6	135.19	10.11			
7	140.5	10.17	31	140.43	9.96
8	145.16	10.03			
9	150.25	9.88	33	149.58	9.94
10	155.21	9.99			
11	160.31	9.98	35	160.19	9.88
12	165.21	10.02			
13	170.22	9.97	37	170.01	9.98
14	175.33	10.04			
15	180.24	9.95	39	180.1	9.84
16	185.45	9.98			
17	190.32	9.89	41	190.12	9.89
18	195.24	9.95			
19	200.23	9.64			
20	205.21	9.42			
21	210.38	9.72	43	211.25	9.77
22	215.28	9.57			
23	220.37	9.57	45	220.63	9.51
24	225.18	9.5			
25	230.3	9.68	47	230.1	9.63
26	235.25	9.8			
27	240.13	9.66	49	240.07	9.63
28	245.15	9.42			
29	250.21	9.36	51	249.73	9.25

30	254.84	9.45			
31	259.85	9.47	55	260.04	9.5
32	265.02	9.45			
33	270.12	9.41	57	270.03	9.41
34	275.17	9.34			
35	280.08	9.33	59	280.01	9.28
36	285.04	9.16			
37	290.22	9.1	61	290.14	9.07
38	295.12	9.1			
39	300.28	8.98	63	300.11	8.97
40	305.36	9.07			
41	310.39	8.97	65	310.3	8.91
42	315.48	8.85			
43	320.37	8.64	67	320.19	8.68
44	325.3	8.6			
45	330.28	8.48	69	330.36	8.4
46	335.38	8.27			
47	340.32	8.25	71	340.12	8.15
48	345.44	8.1			
49	350.44	7.98	73	350.28	7.91
50	355.58	7.85			
51	360.33	7.76	75	360.05	7.73
52	365	7.81			
53	370.31	7.73	77	369.99	7.71
54	374.79	7.79			
55	380.05	7.76	79	380.03	7.77
56	384.82	7.52			
57	390.08	7.51	81	390.17	7.51
58	395.13	7.45			
59	400.12	7.38	83	400.16	7.38
60	404.93	7.3			
61	409.98	7.29	85	410.03	7.2
62	415.17	7.35			
63	420.11	7.39	87	420.1	7.44
64	425.05	7.32			
65	430.03	7.31	89	430.07	7.27
66	435.09	7.37			
67	440.04	7.33	91	440.33	7.27
68	445.02	7.3			
69	449.95	7.35	93	449.79	7.26
70	454.89	7.12			
71	459.99	7.01	95	460.05	6.92
72	465.34	6.89			
73	469.81	6.76	97	469.73	6.69
74	475.02	6.77			
75	480.14	6.9	99	479.99	6.75

76	484.9	6.67			
77	489.96	6.63	101	489.97	6.6
78	495.04	6.76			
79	500.2	6.73	103	500.38	6.64
80	504.9	6.78			
81	510.09	6.67	105	510.25	6.62
82	515.13	6.77			
83	519.95	6.83	107	520	6.87
84	524.72	6.75			
85	529.9	6.62	109	530.11	6.55
86	534.87	6.55			
87	539.62	6.39	111	539.91	6.37
88	544.64	6.37			
89	549.83	6.32	113	549.57	6.29
90	554.92	6.26			
91	559.57	6.15	115	559.88	6.02
92	565.02	6.04			
93	569.97	5.72	117	570.59	5.75
94	574.99	5.87			
95	580.14	5.75	119	580.1	5.81
96	584.83	5.78			
97	589.88	5.46	121	590.3	5.47
98	594.93	5.43			
99	599.9	5.34	123	600.18	5.28
100	604.98	5.31			
101	610.04	5.1	125	610.24	5.2
102	615.03	5.18			
103	620.15	5.1	127	620.5	5.08
104	625.16	5.04			
105	630.17	4.88	129	629.94	4.77
106	635.03	4.6			
107	640.19	4.49	131	639.99	4.4
108	645.35	4.34			
109	649.85	4.37	133	650.2	4.28
110	655.03	4.21			
111	660.25	4	135	659.97	3.92
112	664.82	3.93			
113	669.86	3.68	139	669.8	3.63
114	674.85	3.54			
115	679.6	3.33	141	680	3.52
116	685.2	3.37			
117	690.18	3.47	143	690.13	3.41
118	695.07	3.14			
119	700.03	3.21	163	700.07	3.31
120	705.2	3.3			
			165	710.16	3.1

			167	720.25	2.94
			169	729.85	2.67
			171	739.61	2.22
			173	750.23	2.12
			177	759.9	1.64
			179	769.68	1.05
			181	780.01	1.01
			183	790.07	0.54
			185	810.22	0

Appendix B

Distances and elevations along SG 2 seismic line.
Measurements are relative to first shotpoint at the south end of the line.

Station No.	Receiver Dist. (m)	Receiver Elev. (m)	Station No.	Shot Dist. (m)	Shot Elev. (m)
			1	0	1.08
			3	10.08	0.85
			5	20.23	1
			7	29.64	0.91
			9	39.53	1.23
			13	59.39	0.98
			15	70.05	0.81
			17	79.61	0.51
			19	89.36	0.43
			21	99.39	0.53
23	109.38	0.39	23	109.38	0.39
24	114.58	0.41			
25	119.75	0.42	25	119.75	0.42
26	124.63	0.66			
27	129.78	0.55	27	129.74	0.45
28	134.56	0.64			
29	139.39	0.46	29	139.58	0.39
30	144.62	0.47			
31	149.91	0.47	31	149.11	0.46
32	154.82	0.5			
33	159.89	0.47	33	159.05	0.46
34	164.89	0.61			
35	169.38	1.07	35	169.41	1.02
36	174.35	0.94			
37	179.27	0.56	37	179.44	0.48
38	184.21	0.55			
39	189.32	0.51	39	189.48	0.55
40	194.41	1.27			
41	199.15	0.38	41	199.31	0.39
42	204.4	0.61			

43	209.4	0.69	43	209.29	0.63
44	214.18	0.44			
45	219.14	0.48	45	219.78	0.47
46	224.51	0.28			
47	229.68	0.5	47	229.96	0.17
48	234.35	0.26			
49	239.6	0.14	49	239.62	0.15
50	244.41	0.4			
51	249.59	0.15	51	249.47	0.1
52	254.34	0.35			
53	259.41	0.49			
54	264.37	0.09			
55	269.35	0.65	55	269.26	0.52
56	274.42	0.64			
57	279.64	0.8	57	279.48	0.52
58	284.66	0.51			
59	289.61	0.49	59	289.62	0.43
60	294.68	0.62			
61	299.31	0.91	61	299.43	0.71
62	304.14	1.59			
63	309.44	1.87	63	309.05	1.9
64	314.42	1.77			
65	319.32	2.3	65	319.05	2.09
66	323.86	1.76			
67	329.03	1.34	67	328.78	1.24
68	334.04	0.65			
69	339.25	0.85	69	339.24	0.63
70	344.14	0.74			
71	349.38	0.42	71	348.93	0.49
72	354.28	0.64			
73	359.27	0.39	73	358.59	0.48
74	363.97	0.37			
75	368.9	0.46	75	368.86	0.53
76	374.29	0.46			
77	379.34	0.42	77	379.27	0.43
78	384.48	0.53			
79	389.1	0.05	79	389.15	0
80	394.18	0.42			
81	399.53	0.43	81	399.5	0.48
82	404.61	0.43			
83	409.6	0.53	83	409.53	0.44
84	414.26	0.65			
85	419.36	0.31	85	419.23	0.35
86	424.52	0.32			
87	429.31	0.35	87	429.84	0.34
88	434.24	0.61			

89	439.38	0.96	89	439.62	0.99
90	444.32	1.65			
91	449.04	3.73	91	449.11	3.55
92	453.48	5.88			
93	458.1	7.99	93	458.7	7.7
94	463.32	9.03			
95	468	9.31	95	468.29	9.3
96	472.81	9.45			
97	477.72	9.39	97	477.83	9.3
98	483.23	9.64			
99	488.16	9.68	99	488.29	9.63
100	493.45	9.86			
101	498.29	10.02	101	498.1	9.92
102	503.17	10.27			
103	507.82	10.31	103	508.13	10.28
104	512.64	10.43			
105	518.23	10.63	105	517.93	10.45
106	522.84	10.65			
107	528.28	10.92	107	528.08	10.9
108	532.59	11.01			
109	537.79	11.16	109	537.71	11.02
110	543.28	11.3			
111	547.98	11.32	111	547.98	11.29
112	552.87	11.59			
113	558	11.57	113	557.97	11.53
114	562.88	11.7			
115	568.27	11.97	115	568.03	11.94
116	573.08	12.1			
117	578.04	12.16	117	578.1	12.19
118	583.29	12.48			
119	588.04	12.65	119	588.07	12.6
120	592.88	12.81			
121	597.89	12.97	121	598.07	13.01
122	603.1	13.4			
123	608.35	13.46	123	608.17	13.37
124	613.25	13.63			
125	618.36	13.75	125	618.21	13.74
126	623.14	14			
127	628.05	13.96	127	627.94	13.86
128	633.4	14.17			
129	638.07	14.27	129	638.12	14.19
130	642.8	14.29			
131	648.25	14.6	131	648.22	14.52
132	653.27	14.5			
133	657.95	14.27	133	658.07	14.24
134	663.17	14.66			

135	668.2	15.24	135	668.24	15.26
136	673.29	15.71			
137	678	15.98			
138	683.28	15.53			
139	688.29	15.72	139	688.13	15.67
140	693.36	15.78			
141	698.37	15.9	141	698.31	15.93
142	703.15	16.06			
143	708.15	18	143	707.66	16.46
144	713.15	18			
145	718.15	18			
146	723.15	18			
147	728.15	18			
148	733.15	18			
149	738.15	18			
150	743.15	18			
151	748.15	18			
152	753.15	18			
153	758.15	18			
154	763.15	18			
155	768.15	18			
156	773.15	18			
157	778.15	18			
158	783.15	18			
159	788.15	18			
160	793.15	18			
161	798.15	18			
162	803.15	18			
163	808.15	18	163	810.54	20.48
164	815.13	20.59			
165	820.4	20.64	165	820.52	20.58
166	825.36	20.67			
167	830.31	20.91	167	830.47	20.8
168	835.35	21.15			
169	840.41	21.36	169	840.33	21.3
170	845.4	21.54			
171	850.48	21.73	171	851	21.74
172	855.39	21.92			
173	860.39	22.22	173	860.64	22.14
174	865.42	22.4			
175	870.22	22.64			
176	875.47	22.8			
177	880.33	23.02	177	880.23	22.95
178	885.3	23.02			
179	890.28	23.45	179	890.34	23.25
180	895.23	23.71			

181	900.27	23.93	181	900.35	23.77
182	905.51	24.25			
183	910.38	24.47	183	910.38	24.32
184	915.32	24.7			
185	920.37	24.89	185	920.4	24.89
186	925.33	25.11			
187	930.26	25.34	187	930.38	25.17
188	935.26	25.61			
189	940.21	25.8	189	940.21	25.74
190	945.22	25.94			
191	950.2	26.21	191	950.21	26.24
192	955.23	26.45			
193	960.16	26.72	193	959.94	26.61
194	965.31	26.85			
195	970.19	27.06	195	970.32	26.91
196	975.27	27.19			
197	980.16	27.38	197	980.13	27.33
198	985.11	27.53			
199	990.25	27.72	199	990.45	27.59
200	995.1	27.93			
201	999.99	28.18	201	999.9	27.95
202	1005.28	28.41			
203	1010.13	28.69	203	1010.07	28.6
204	1015.31	28.96			
205	1020.19	29.21	205	1020.19	29.14
206	1025.19	29.37			
207	1030.31	29.62	207	1030.2	29.5
208	1035.14	29.75			
209	1040	29.88	209	1040.17	29.88
210	1045.06	30.14			
211	1050.08	30.3	211	1050.1	30.32
212	1055.1	30.65			
213	1059.9	30.96	213	1059.77	30.96
214	1064.91	30.89			
215	1070.14	31.17	215	1070.09	31.07
216	1075.08	31.36			
217	1079.71	31.71	217	1079.79	31.71
218	1084.86	31.93			
219	1089.94	32.18	219	1089.97	32.18
220	1095	32.41			
221	1099.89	32.57	221	1099.77	32.56
222	1105.44	32.71			
223	1110.05	32.95	223	1109.98	32.85
224	1115.25	33.2			
225	1119.9	33.58	225	1120.13	33.34
226	1124.71	33.85			

227	1129.89	34.06	227	1129.63	33.92
228	1134.77	34.39			
229	1139.6	34.59	229	1139.68	34.4
230	1144.65	34.69			
231	1149.89	35.09	231	1149.67	35.04
232	1154.55	35.33			
233	1159.73	35.56	233	1160.02	35.43
234	1164.67	35.83			
235	1169.83	36.03	235	1169.8	35.9
236	1174.43	36.2			
237	1179.63	36.28	237	1179.3	36.27
238	1184.51	36.57			
239	1189.5	36.84	239	1189.43	36.6
240	1194.31	36.93			
241	1199.07	37.06	241	1198.89	36.93
242	1203.98	37.32			
243	1209.45	37.57	243	1209.21	37.36
244	1214.17	37.81			
245	1218.92	38.04	245	1218.87	37.88
246	1224.1	38.4			
247	1229.1	38.54	247	1229.22	38.55
248	1234.05	38.88			
249	1239.17	39.06	249	1238.84	38.97
250	1243.84	39.3			
251	1248.74	39.47	251	1248.69	39.47
252	1253.87	39.73			
253	1258.65	39.98	253	1258.85	39.93
254	1263.71	40.27			
255	1268.58	40.45	255	1268.85	40.35
256	1273.59	40.72			
257	1278.84	41.02	257	1278.83	40.89
258	1283.4	41.33			
259	1288.59	41.61	259	1288.33	41.33
260	1293.32	41.81			
261	1298.7	42.14	261	1298.57	41.95
262	1303.28	42.31			
263	1308.25	42.52	263	1307.69	42.49
264	1313.48	42.79			
265	1318.18	42.97	265	1318.1	42.89
266	1323.39	43.08			
267	1328.77	43.37	267	1328.94	43.45
268	1333.81	43.67			
269	1338.73	43.88	269	1338.81	43.8
270	1343.49	44.28			
271	1348.38	44.48	271	1348.35	44.37
272	1353.21	44.99			

273	1358.4	45.42	273	1358.16	44.85
274	1363.3	46			
275	1368.18	46.25	275	1368.27	45.44
276	1373.11	46.88			
277	1378.01	46.54	277	1378.23	46.66
278	1382.99	46.92			
279	1387.65	47.49	279	1387.91	47.77
280	1392.4	47.91			
281	1397.59	48.38	281	1397.55	48.87
282	1402.3	49.05			
283	1407	49.76	297	1477.36	51.47
			301	1497.81	52.18
			303	1507.31	52.79
			307	1527.77	53.87
			309	1537.37	54.5
			315	1566.98	56.19
			317	1577.45	56.69